Title Page

Potential role of PRKCSH in lung cancer: Bioinformatics analysis and a case study of Nano ZnO

Ridan Lei[1#], Meiling Zhou[1], Shusheng Zhang[2#], Jinhua Luo[1], Can Qu[1], Yin Wang[1], Peiyu Guo[1], Ruixue Huang[1*]

[1]Department of Occupational and Environmental Health, Xiangya School of Public Health, Central South University, Changsha, Hunan Province 410078, China Tel: 0086-731-84805460, 173850711@qq.com(RD L); huangruixue@csu.edu.cn(RX H); 1027267855@qq.com(ML Z); 2933598163@qq.com(C Q); 2959165855@qq.com(Y W); luojinhua@csu.edu.cn(JH L); 1484636625@qq.com（PY G）

2 Changsha Stomatological Hospital, Changsha, Hunan Province, China. 2680329408@qq.com(SS Z)

[#] Ridan Lei and Shusheng Zhang contributed equally to this study.

Correspondence:

*Correspondence: Ruixue Huang, Department of Occupational and Environmental Health, Xiangya School of Public Health, Central South University, Changsha, Hunan Province 410078, China Tel: 0086-731-84805460,huangruixue@csu.edu.cn(RX H)

Running title: PRKCSH and Nano ZnO

Abstract

PRKCSH, also known as glucosidase II beta, functions as a contributor to lung tumorigenesis by regulating the cell cycle in a p53-dependent manner under severe environmental stress. However, the prognostic value and molecular mechanisms by which the level of PRKCSH is significantly increased in cancer cells are not clearly understood. Here, we first generated a biological profile of PRKCSH expression changes in cancers by analyzing bioinformatic data from cancer databases. We found that higher PRKCSH expression was correlated with a poorer prognosis and greater infiltration of most immune cell types in patients with lung cancer. In particular, PRKCSH expression showed significant negative correlations with the level of STAT6 ($r = -0.31$, $p < 0.001$) in lung cancer tissues. We further found that PRKCSH deficiency promoted G2/M arrest in response to zinc oxide nanoparticle (Nano ZnO) treatment in A549 cells. With regard to the mechanism, PRKCSH deficiency may induce STAT6 translocation to the nucleus to activate p53 expression through binding to the p53 promoter region from −365 bp to +126 bp. Eventually, activated p53 contributed to Nano-ZnO-induced G2/M arrest in lung cancer cells. Taken together, our data provide new insights into immunotherapy target choices and the prognostic value of PRKCSH. Since the G2/M cell cycle checkpoint is crucial for lung cancer prognosis, targeting PRKCSH expression to suppress the activation of the STAT6/p53 pathway is a potential therapeutic strategy for managing lung cancer.

Keywords: lung cancer; nanomaterial; cell cycle; p53; signalling pathway

Introduction

Approximately 2 million people worldwide are diagnosed with lung cancer every year, and approximately 1.6 million people die from the disease [1]. Regional factors and cancer stage influence the disease 5-year survival rate, which ranges from 4% to 17% [2]. Current therapeutic strategies include surgery, chemotherapy, radiotherapy, and immunotherapy [3]. Recent research has shown that nanoparticles (NPs) can inhibit some cancers and may be used to deliver anticancer drugs [4]. For instance, zinc oxide nanoparticle (Nano ZnO) treatment has promising anticancer activity [5]. Although new treatments have improved the prognoses of many patients with lung cancer, there are still clinical challenges, such as resistance to chemotherapy and radiotherapy. For example, patients with stage IA lung cancer have a better 5-year survival rate (77–92%) than those with stage IIB lung cancer (53%) [6]. However, for those with advanced non-small-cell lung cancer (NSCLC) who cannot be treated by surgical resection, there is no targeted treatment that can be combined effectively with current chemotherapy and radiotherapy regimens, and multi-centre trials have reported a 5-year survival rate of only 15–20% for these patients [7]. Lung cancer development and progression are influenced by the immunological microenvironment. However, most previous immunotherapy approaches have focused on vaccines such as TG4010, which have been ineffective [8]. Consequently, a better understanding of how key genes interact with immune cells may be necessary to improve lung cancer therapies.

Protein kinase C substrate 80K-H (PRKCSH), also known as glucosidase IIβ, is located in the endoplasmic reticulum (ER) and interacts with glucosidase IIα in *N*-glycan processing. Mutations in PRKCSH may lead to autosomal-dominant polycystic liver disease [9]. PRKCSH stimulates tumorigenesis in some cancers via selective activation of the inositol-requiring enzyme 1α signalling pathway [10]. Increased PRKCSH expression is positively correlated with the progression of lymph node metastasis in breast cancer [11]. PRKCSH is reportedly associated with resistance to chemotherapeutic drugs such as gefitinib via an unidentified molecular mechanism, and silencing PRKCSH induces the apoptosis of NSCLC cells treated with gefitinib [12]. In addition, PRKCSH expression in patients with lung cancer is influenced by p53 status. The suppression of PRKCSH gene expression results in the autophagy and apoptosis of lung-cancer-derived cells [13]. We previously reported that

PRKCSH expression increased in response to silica-induced epithelial–mesenchymal transition and that the knockdown (KD) of a PRKCSH-2 splice variant stimulated A549 cell proliferation by promoting epithelial–mesenchymal transition [14]. It remains unclear whether PRKCSH interacts with lung cancer immune infiltration-related signalling pathways and/or whether this affects lung cancer proliferation or prognosis.

Nano ZnO is a material that is widely used for industrial purposes and has the potential for use in biomedical and cancer applications [15]. Compared to chemotherapeutic agents, Nano ZnO exhibits a high degree of cancer cell selectivity with the capacity to surpass therapeutic indices [16]. The special property of Nano ZnO for selective cytotoxicity is mainly attributed to its ability to induce reactive oxygen species (ROS) production or activate the ER stress-responsive pathway [17] or induce cell cycle arrest at the G2/M phase [18] and eventually lead to cancer cell death [19]. P53, one of the most extensively studied cancer and environmental stress-related adaptive proteins in the past four decades [20], plays a role in NP-induced G2/M arrest. For instance, Ye BL et al found that chitosan-coated doxorubicin NPs inhibited liver cancer cell growth by arresting the cell cycle at the G2/M phase through the p53/PRC1 pathway [21]. Another study showed that benzofuran-pyrazole NPs could induce pre-G1 apoptosis and cell cycle arrest at the G2/M phase by upregulating p53 expression [22]. It has also been reported that in p53+/+ cells, signal transducer and activator of transcription 6 (STAT6) was activated, while there was no significant change in p53-deficient cells, suggesting that p53 status can affect cell immune-related cytokine expression [23]. However, the association among p53, PRKCSH and STAT6 and the role of p53 in Nano-ZnO-induced G2/M arrest as well as the underlying mechanisms remain unclear.

In this study, we analysed the expression of PRKCSH and its correlation with the prognoses of various cancers, including lung cancer. We also evaluated the status of different cancer-infiltrating immune cells by performing a meta-analysis of data from the ONCOMINE, Kaplan–Meier plotter, Gene Expression Profiling Interactive Analysis (GEPIA), and Tumor Immune Estimation Resource (TIMER) databases. We found that the expression of PRKCSH was negatively correlated with the expression of STAT6 in lung cancer tissues and cell lines. Survival analyses showed that the overexpression of PRKCSH was associated with a poor prognosis. Finally, we found evidence that PRKCSH deficiency stimulated the translocation

of STAT6 from the cytoplasm to the nucleus, where it bound competitively to p53, inducing G2/M arrest in A549 cells.

Results

1. PRKCSH mRNA expression is increased in cancerous tissues

Previous studies demonstrated that PRKCSH stimulated tumorigenesis [10] and that a PRKCSH splice variant was important for epithelial–mesenchymal transition and cell proliferation [14]. We investigated PRKCSH mRNA expression in cancerous and normal tissues using the online GEPIA database. Compared with the corresponding normal tissues, PRKCSH mRNA levels were significantly higher in tissues affected by leukaemia or by brain, lung, colorectal, ovarian, or sarcoma cancers (Fig. 1A). We also used The Cancer Genome Atlas (TCGA) online database to evaluate RNA sequences from the ONCOMINE and TIMER databases. Compared with the corresponding normal tissues, PRKCSH mRNA levels were significantly higher in the following tissues: bladder urothelial carcinoma, breast invasive carcinoma, cholangiocarcinoma, colon adenocarcinoma, oesophageal carcinoma, head and neck cancer, head and neck cancer with human papillomavirus infection, kidney chromophobe, renal clear cell carcinoma, kidney renal papillary carcinoma, hepatocellular carcinoma, lung adenocarcinoma (LUAD), lung squamous cell carcinoma, prostate adenocarcinoma, rectum adenocarcinoma, stomach adenocarcinoma, and uterine corpus endometrial carcinoma (Fig. 1B–C). These results suggest that PRKCSH expression plays an important role in the development and progression of various cancers.

2. The clinical prognostic value of PRKCSH expression may depend on the cancer type

As described above, PRKCSH is overexpressed in various cancer tissues. We analysed the prognostic value of PRKCSH expression in various cancers using the Kaplan–Meier plotter database (http://kmplot.com/). Changes in PRKCSH expression were associated with a poorer prognosis in terms of the following: overall survival (OS) (hazard ratio [HR]=1.3, 1.14-1.48, p<0.01) and first progression survival (FP) (HR=2.01, 1.65-2.45, p<0.01), but no significant effect on postprogression survival (PPS) (HR=0.87, 0.68-1.13, p=0.3), in LUAD (Fig. 1D); disease-free survival (DFS) (HR: 1.79, $p = 0.0007$) in adrenocortical carcinoma; OS (HR: 1.1, $p = 0.4$) and DFS (HR: 1.2, $p = 0.26$) in bladder urothelial carcinoma; OS (HR: 1.58, $p = 0.0003$) and PPS (HR: 3.13, $p = 0.0001$) in stomach adenocarcinoma; and OS (HR:

2.5, p = 0.19) and DFS (HR: 1.3, p = 0.17) in prostate adenocarcinoma (Supplementary Figure. 1A). However, changes in PRKCSH expression were not associated with the following prognoses: distant metastasis-free survival (HR: 1.06, p = 0.62), PPS (HR: 0.88, p = 0.11), OS (HR: 0.78, p = 0.0086), and DFS (HR: 0.91, p = 0.078) in breast invasive carcinoma; OS (HR: 0.74, p = 0.53) and DFS (HR: 1.5, p = 0.43) in cholangiocarcinoma; OS (HR: 0.94, p = 0.81) and DFS (HR: 0.97, p = 0.9) in colon adenocarcinoma; OS (HR: 0.85, p = 0.48) and DFS (HR: 0.83, p = 0.44) in oesophageal carcinoma; OS (HR: 0.75, p = 0.42) and DFS (HR: 0.95, p = 0.87) in uterine corpus endometrial carcinoma; distant metastasis-free survival (HR: 0.66, p = 0.071), PPS (HR: 0.86, p = 0.37), OS (HR: 0.82, p = 0.27), and DFS (HR: 0.81, p = 0.15) in hepatocellular carcinoma; and DFS (HR: 0.87, p = 0.032), PPS (HR: 0.95, p = 0.53), and OS (HR: 0.81, p = 0.21) in epithelial ovarian cancer (Supplementary Figure 1B–C and Supplementary Figure 2A–F). Therefore, PRKCSH overexpression may have clinical prognostic significance for only select cancers (e.g., adrenocortical carcinoma, bladder urothelial carcinoma, stomach adenocarcinoma, and LUAD). Furthermore, the degree of correlation between PRKCSH expression and clinical prognosis may also depend on the type of cancer.

3. Alterations in PRKCSH expression have prognostic value in lung cancer

We used the Kaplan–Meier plotter database to investigate the association between PRKCSH expression and prognosis and various clinical characteristics in patients with lung cancer (Table S1). The overexpression of PRKCSH was correlated with poorer overall survival in females (HR = 1.34, p = 0.016); patients with stage I (HR = 1.8, p < 0.001), stage II (HR = 1.88, p < 0.001), or grade II (HR = 1, p < 0.001) cancer; patients with adenocarcinoma (HR = 1.83, p < 0.001); and patients with a history of smoking (HR = 2.43, p < 0.001). These results demonstrate that the prognostic significance of PRKCSH expression in patients with lung cancer was affected by clinical characteristics such as sex, cancer stage, the presence of adenocarcinoma, and smoking history.

4. PRKCSH expression is correlated with immune cell infiltration in patients with lung carcinoma

Previous studies have reported that the survival time of cancer patients depends on the quantity and activity of tumour-infiltrating lymphocytes [24, 25]. Therefore, we used the

TIMER database to investigate the association between PRKCSH expression and immune cell infiltration in various types of cancer. We found that PRKCSH expression levels in bladder urothelial carcinoma, breast invasive carcinoma, LUAD, and lung squamous cell carcinoma cancer tissues were negatively correlated with tumour purity and the infiltration of B cells, $CD8^+$ T cells, $CD4^+$ T cells, macrophages, neutrophils, and dendritic cells (Fig. 2A–D and Table S3, Supplementary Figure 3A-E and Supplementary Figure 4A-B and Supplementary Figure 5). In addition, we investigated correlations between PRKCSH expression and immune cell infiltration and prognoses in patients with lung cancer and stomach adenocarcinoma using the GEPIA database, which has six major analytic modules used to evaluate associations between immune infiltration and factors such as gene expression and mutations [26, 27]. Higher PRKCSH expression was correlated with a poorer prognosis and greater infiltration of most immune cell types in patients with lung cancer and stomach adenocarcinoma (Fig. 3A–F and Table S4). PRKCSH expression showed significant positive correlations with the levels of ISYNA1 ($r = 0.3$, $p < 0.001$), GATA3 ($r = 0.13$, $p < 0.001$), STAT5A ($r = 0.11$, $p < 0.001$), STAT3 ($r = 0.25$, $p < 0.001$), and STAT5B ($r = 0.18$, $p < 0.001$) in LUAD tissues (Table S4). PRKCSH expression was negatively correlated with the expression of STAT6 ($r = -0.31$, $p < 0.001$) and human leukocyte antigen-DR α-chain ($r = 0.16$, $p < 0.001$) in LUAD tissues. Notably, the most significant correlation was between the expression levels of PRKCSH and STAT6, a marker of T helper 2 (Th2) cells. Similar correlations were observed in patients with stomach adenocarcinoma (Table S4). These data suggest that PRKCSH expression modulates the infiltration of immune cells into tumour tissues. In addition, PRKCSH and STAT6 may have important functions in lung cancer. Based on these results, we hypothesized that the molecular mechanism of PRKCSH function may be associated with STAT6.

5. PRKCSH is upregulated and STAT6 is downregulated in lung cancer cells, *and PRKCSH deficiency leads to the inactivation of the G2/M checkpoint*

The database analyses described above suggested that PRKCSH and STAT6 levels are potential prognostic indicators for patients with lung cancer. Therefore, we investigated the functions of PRKCSH and STAT6 in cancer cells using the online Human Protein Atlas database (https://www.proteinatlas.org/). PRKCSH was expressed more strongly than STAT6

in various cancer tissues (Fig. 4A). Immunofluorescence staining of a human cancer cell line showed that STAT6 was found mainly in the nucleoplasm and cytosol, whereas PRKCSH was found mainly in the ER (Fig. 4B). Nano ZnO is a widely used material. Chen R et al found that Nano ZnO could induce a significant cellular ER stress response, indicating that Nano ZnO activates the ER stress-responsive pathway and that the ER stress response might be used as an earlier and more sensitive end point for nanotoxicological studies [17].

Further analyses showed that the STAT6 and PRKCSH levels were highest in macrophages and fibroblasts, respectively (Fig. 4C). Correlation analyses indicated a positive relationship between the levels of STAT6 and p53 in lung cancer cells (Fig. 4D). STAT6 was identified as a favourable prognostic marker for patients with lung cancer (HR=0.68, 0.6-0.78, p<0.01) using the Kaplan–Meier plotter database (Fig. 4E), whereas PRKCSH (Fig. 1D) and p53 (Fig. 4F) were unfavourable prognostic markers for patients with lung cancer (HR=1.39, 1.22-1.58, p<0.01). We used the online Human Protein Atlas database to compare the expression of STAT6 and PRKCSH in normal lung and lung cancer tissues. Immunohistochemical staining showed that PRKCSH expression was stronger (Fig. 5A) and more frequently altered (Fig. 5B–C) than STAT6 expression in lung cancer tissue. In patients with lung cancer, the type of genetic alteration of PRKCSH was amplification whereas that of STAT6 was deep deletion in comparison to healthy controls (Fig. 5D–E) (http://www.cbioportal.org/). Patients with lung cancer with altered PRKCSH expression had poorer OS rates (34.33, 95% confidence interval, 11.27–not applicable [NA]) than those with altered STAT6 expression (48.01, 95% confidence interval, 41.88–NA; Fig. 5F–G). These results indicate increased PRKCSH expression and decreased STAT6 expression in lung cancer cells. In addition, changes in PRKCSH expression may be associated with a specific function of STAT6.

6. PRKCSH deficiency promotes G2/M arrest via STAT6 phosphorylation in response to Nano ZnO

To further explore the regulatory molecular mechanism of PRKCSH and STAT6 in lung cancer, in particular the role of PRKCSH function in response to external environmental factors such as NPs, we used Nano ZnO in further studies [17]. The characterization of Nano ZnO is shown in Supplementary Figure 6A-C. The size of Nano ZnO was determined to be

30-70 nm. The G2/M cell cycle checkpoint is critical for maintaining genomic stability. Many cancer cells lack functional p53 at the G1/S checkpoint. Therefore, the G2/M checkpoint is particularly critical for the cancer cell cycle and for cancer prognosis [28]. The expression of PRKCSH was dose- and time-dependent after Nano ZnO treatment (Fig. 6A-B). The proportions of G2- and M-phase cells increased in a time-dependent manner after treatment with 30 μg/mL Nano ZnO, showing that G2/M and/or mitosis was arrested in PRKCSH-wild-type (WT) lung cancer cells, whereas PRKCSH-KD lung cancer cells exhibited higher proportions of cells in the G2 and M phases (Fig. 6C–D). No significant G2/M arrest was observed in A549 cells treated with or without Nano ZnO (Supplementary Figure 6D). After treatment with Nano ZnO, phospho-histone H3 expression was higher in PRKCSH-KD cells than in PRKCSH-WT cells (Fig. 6E–F). These results show that PRKCSH deficiency leads to the activation of the G2/M checkpoint in response to Nano ZnO in lung cancer cells. To further investigate the role of PRKCSH in Nano-ZnO-induced G2/M arrest, we measured the levels of DNA damage repair-related proteins in PRKCSH-WT and PRKCSH-KD cells after treatment with Nano ZnO. As shown in Fig. 6G, there were no significant alterations in the levels of p-DNApkcs, p-ATM, p-ATR, KAP1, p-CHK1, p-CHK2, or pRPA2 in A549 cells; however, the expression of p53 and p-STAT6 was increased in PRKCSH-KD cells. STAT6 was phosphorylated and activated in PRKCSH-KD cells following treatment with Nano ZnO (Fig. 6G, Supplementary Figure 7A). These results suggest that PRKCSH deficiency stimulates the phosphorylation of STAT6 and the G2/M checkpoint is activated by PRKCSH deficiency or the activation of the STAT6/p53 signalling pathway.

7. PRKCSH deficiency promotes a specific interaction between STAT6 and p53 in response to Nano ZnO

Previous research showed that interleukin (IL)-4 deficiency resulted in STAT6 phosphorylation and translocation from the cytoplasm to the nucleus, inducing DNA damage [29]. Therefore, we investigated the interaction between STAT6 and p53 after PRKCSH KD. After treatment with Nano ZnO, the level of phosphorylated STAT6 in PRKCSH-KD cells increased, probably due to the inactivation of PRKCSH (Fig. 7A, Supplementary Figure 7B). We also determined the changes in apoptosis and cell cycle arrest induced by Nano ZnO in p53-silenced cells or non-p53-expressing cells. As shown in Supplementary Figure 8A-B,

compared with the p53-WT A549 cells, the number of apoptotic cells decreased and the number of G2 cells decreased in p53-knockout A549 cells after treatment with Nano ZnO. Bax and Bcl-2 expression, which are downstream genes in the p53 pathway, was increased in PRKCSH-KD cells compared with PRKCSH-WT cells after treatment with Nano ZnO (Supplementary Figure 9A). After Nano ZnO treatment, the cytoplasmic STAT6 level decreased in PRKCSH-WT cells, but Nano-ZnO-induced translocation of STAT6 from the cytoplasm to the nucleus was stimulated in PRKCSH-KD cells (Fig. 7B). Coimmunoprecipitation (coIP) assays showed that the KD of STAT6 in A549 cells enhanced the binding of endogenous murine double minute 2 homologue to p53 (Fig. 7C). Moreover, the coIP results indicated that the interaction between STAT6 and p53 increased after Nano ZnO treatment in PRKCSH-KD cells, showing that PRKCSH influenced the interaction between STAT6 and p53 (Fig. 7D). Immunofluorescence staining also demonstrated that the translocation of STAT6 from the cytoplasm to the nucleus was enhanced in PRKCSH-KD cells treated with Nano ZnO (Fig. 8A). In addition, we found that the KD of STAT6 resulted in decreased levels of p53 and phosphorylated STAT6 in A549 cells treated with Nano ZnO (Fig. 8B–C). To determine whether STAT6 and p53 interact directly, we performed luciferase assays. The promoter sequence of the p53 gene was analysed, and five potential STAT6-inducible elements were identified using a promoter prediction website (http://alggen.lsi.upc.es/cgi-bin/promo_v3/promo/promo.cgi?dirDB=TF_8.3&idCon=163629015700&getFile=factors/278.html). Serial deletions of the p53 gene promoter were generated and evaluated using luciferase reporter assays to determine the regulatory region that responds to STAT6. We found that the p53 promoter region from −365 bp to +126 bp increased the response to STAT6 stimulation. A mutation in this STAT6-inducible element (i.e., a change from AATTTC to AATGGC) significantly decreased the level of luciferase activity induced by STAT6 (Fig. 8D–E). This suggests that STAT6 activates the transcription of p53 by binding to the p53 promoter. Taken together, our results suggest that PRKCSH is involved in regulating the Nano-ZnO-induced G2/M checkpoint by promoting the interaction between STAT6 and p53 when PRKCSH is deficient. We believe that the PRKCSH–STAT6–p53 axis may be crucial for regulating G2/M arrest in cancer cells treated with Nano ZnO.

Discussion

Increasing evidence indicates that infiltrating immune cells and the G2/M-phase transition associated with DNA damage repair signalling are important in the development and prognosis of cancers [30-32]. The PRKCSH gene encodes the β subunit of glucosidase II, which is needed for the folding and quality control of glycoproteins in ER stress, but the effects of PRKCSH expression on the prognosis of various cancers remain unclear. Here, in this study, the following main findings were obtained: (i) Through comprehensive analysis of multiple online cancer-related databases, including TCGA, we found that PRKCSH expression was increased in cancerous tissues, particularly lung cancer tissues. Higher PRKCSH expression was correlated with a poorer prognosis and greater infiltration of most immune cell types in patients with lung cancer. (ii) PRKCSH deficiency promoted G2/M arrest via STAT6 phosphorylation in response to Nano ZnO.

Worapong K et al reported that suppressing the expression of the Glullβ-encoding gene PRKCSH by bromoconduritol led to the induction of autophagy and decreased the activation of the EGFR/RTK and PI3K/AKT signalling pathways in lung cancer cells [13]. Another report indicated that silencing PRKCSH induced apoptosis in NSCLC cells treated with gefitinib, suggesting that PRKCSH may prevent lung cancer cell death [12]. Liu H et al identified that low expression of PRKCSH was related to good prognosis in LUAD via RNA-sequencing (RNA-seq) detection [33]. Our results based on the comprehensive analysis of the TCGA lung cancer database are consistent with these previous reports, in which increased PRKCSH mRNA expression was associated with a poorer prognosis in lung cancer. These findings are consistent with other previous reports, suggesting that PRKCSH expression plays an important role in the development of lung cancers [10]. In this study, the results indicate that Nano ZnO is more toxic to normal cells than to tumour cells, which may be due to the dose of Nano ZnO, the different cell lines or some essential genes, such as p53. Dose is a very important factor. As Chen Fangchuan et al showed, ZnO NPs did not affect human gingival cell proliferation at low concentrations, but high concentrations of Nano ZnO inhibited cell proliferation, destroyed the integrity of cell membranes, and induced oxidative stress and apoptosis [34]. Nano ZnO has also been reported to exhibit selective cytotoxicity through zinc-mediated protein disequilibrium and oxidative stress. According to Steffy Thomas et al,

Nano ZnO shows good inhibitory activity by decreasing the viability of cancerous cells in a dose- and time-dependent manner [5]. Lucian F et al tested the toxicity of a panel of representative oxide nanomaterials on normal and cancer cells and indicated that macrophages were the cell type most sensitive to short-term exposure (24-72 h) ($ZnO>SiO_2>TiO_2$)[35]. However, the findings from our current study should be further investigated and verified in other cancer cells or normal cells in the future.

Recent studies have reported that greater levels of T and B cell infiltration in patients with NSCLC were associated with better prognoses [36]. An increased level of $CD8^+$ T cells was associated with increased survival in patients with LUAD [37]. Some studies reported that the infiltration of dendritic cells was associated with increased protective immunity in patients with LUAD [38]. For example, high CKS2 expression was associated with a poor prognosis and was correlated with low levels of infiltrating $CD8^+$ T cells, $CD4^+$ T cells, natural killer cells, B cells, and dendritic cells [39]. Tubeimoside-1 had beneficial effects on mice with lung cancer by activating tumour-infiltrating T cell immunity [40]. Cancer prognostic models have been developed based on immune-related genes or molecular alterations at various stages of NSCLC; these models predicted better prognoses in patients with greater levels of infiltrating B cells, activated $CD8^+$ T cells, activated dendritic cells, and $CD56^+$ natural killer cells [41]. In this study, we found that PRKCSH expression was decreased in infiltrating immune cells but increased in fibroblasts, whereas STAT6 expression was increased in macrophages. STAT6 belongs to the STAT family of proteins, which are involved in regulating the cell cycle, cell adhesion, apoptosis, and DNA damage signalling. Activated STAT proteins dissociate, undergo dimerization in the cytoplasm, and translocate to the nucleus [42]. STAT6 is involved in IL-4 and IL-13 signalling and plays a key role in Th2 polarization in the immune system [43]. STAT6 is also involved in immune checkpoint blockade and in the immune infiltration of B cells, $CD4^+$ T cells, neutrophils, macrophages, and dendritic cells [44]. Some studies found that STAT6 deficiency decreased the mobilization and differentiation of $CD11b^+$ cells, resulting in the inhibition of cancer growth and improved prognoses [45]. Constitutive activation of STAT6 occurs in various diseases, including T cell lymphoma [46]. Some studies reported that STAT6 activation occurred in IL-4/Luc/CNS-1 transgenic mice treated with 4% phthalic anhydride, leading to decreased

cancer volumes, a reduced allergic response, and natural killer cell activation. Therefore, STAT6 activation may inhibit cancer development [43]. In this study, we found that STAT6 expression was decreased in lung cancer tissue, which is consistent with the results of a previous study [47]. However, we found that PRKCSH expression was increased in lung cancer cells. We also found that STAT6 was a favourable prognostic marker for various cancers. Correlation analyses showed that the relationship between PRKCSH and STAT6 expression was more pronounced in normal tissues than in LUAD tissues. This finding highlighted the importance of the immune tumour microenvironment in the regulation of STAT6 and PRKCSH expression. Therefore, in future studies, the underlying mechanism of the regulation of STAT6 and PRKCSH expression should be investigated.

The G2/M cell cycle checkpoint is crucial for cancer prognoses. Nano ZnO induces hepatotoxicity and the upregulation of ER-associated genes [48]. Nano ZnO can stimulate apoptosis, leading to the destruction of cancer cells [5]. A better understanding of how cancer cells respond to Nano ZnO may lead to better clinical therapeutic strategies and prognoses. A recent study showed that Nano ZnO promotes liver cancer cell apoptosis by inducing autophagy and stimulating p53 [49]. Nano ZnO can inhibit cancer cell nucleotide excision repair, base excision repair, and oxidative damage by DNA glycosylases [50]. Nano ZnO can also inhibit mitotic cell division and induce G2/M arrest in HT-29 cells [51] and cervical cancer cells [18]. Our results are consistent with those reported previously. We found that Nano ZnO induced G2/M arrest in lung cancer cells that exhibited decreased PRKCSH expression. The interactions among PRKCSH, STAT6, and p53 are probably responsible for regulating the G2/M checkpoint in lung cancer cells. Indeed, p53 status would affect NP toxicity. As reported by Masoumeh E et al, the toxicity of Gemini-Cur on p53-WT HCT116 cells and p53-mutant HT29 cells was different. Apoptotic cells were increased in HCT116 cells compared with HT29 cells [52]. Another study found that the PRKCSH inhibition that led to apoptosis in lung-carcinoma-derived cells appeared to be p53 dependent, indicating that the expression status of both genes could be considered in treatment [13]. Upon treatment with Nano ZnO in lung cancer cells, STAT6 is activated and then translocates to the nucleus, where it interacts with p53 to induce G2/M arrest. Our study demonstrates that PRKCSH deficiency may have the potential to induce STAT6 translocation to the nucleus to activate

p53 expression, resulting in Nano ZnO induction of G2/M arrest in lung cancer cells (Fig. 8F). Additional research, such as using PRKCSH knockout mice or STAT6 knockout mice, to further verify this finding should be performed in the future.

Typically, under Nano ZnO exposure, there were indeed some indications of an association among PRKCSH deficiency, STAT6 translocation and p53 activation. However, the consequences of Nano ZnO exposure are complex and not just a manifestation of ER stress. For instance, Xia Y et al indicated that signalling pathway-related oxidative stress and ER stress-induced apoptosis are involved in Nano-ZnO-induced hepatotoxicity in mice [48]. Xiao L et al reported that Nano ZnO may trigger NF-κB-mediated signalling in A549 cells [53]. Wang CX et al demonstrated that Nano ZnO may regulate intracellular ROS-related signalling in human LUAD cells [54]. These findings suggest that other signalling pathways may be involved under Nano ZnO treatment. In addition, there are analogous signalling pathways regulating STAT6/p53 expression in lung cancer. For instance, the inhibitory effects of chitinase 3-like 1 on lung cancer are associated with STAT6-dependent M2 polarization inhibition [55]. A recent study found that targeting the Th2-STAT6-C3-NET (neutrophil extracellular trap) signalling axis effectively inhibited breast cancer metastasis to the lungs [56]. Another study reported that p53 mutations may promote malignancy in solitary fibrous tumours by regulating the NAB2-STAT6 fusion gene at the transcriptional level [57]. Thus, in the future, other signalling pathways regulated by PRKCSH or Nano ZnO in lung cancer should be investigated further.

Conclusions

In summary, we generated a biological profile of PRKCSH expression changes in cancers by analysing bioinformatic data from cancer databases and the relationship between PRKCSH and STAT6 expression. Furthermore, we demonstrated that PRKCSH deficiency may induce STAT6 translocation to the nucleus, which may activate p53 expression and result in Nano-ZnO-induced G2/M arrest in lung cancer cells. The G2/M cell cycle checkpoint is crucial for lung cancer prognosis, and targeting PRKCSH expression to suppress the activation of the STAT6/p53 pathway is a promising therapeutic strategy for managing lung cancer. Furthermore, our findings highlight other molecular targets that are potentially useful for providing improved therapies and more accurate prognoses for patients

with lung cancer. However, additional research, such as using PRKCSH knockout mice or STAT6 knockout mice, to further verify this finding should be performed in the future.

Materials and Methods

Data collection and databases

PRKCSH and STAT6 mRNA expression in various cancers was evaluated using the ONCOMINE database (https://www.oncomine.org/resource/login.html). Expression levels with a 1.5-fold change and p value < 0.001 were considered significant. Analyses of PRKCSH and STAT6 expression and survival rates were performed using the Kaplan–Meier plotter database (http://kmplot.com/analysis/). The results are presented as HRs and log-rank p values. The TIMER database was used to analyse tumour-infiltrating immune cells in various cancer types based on more than 10,000 samples from the TCGA database (https://cistrome.shinyapps.io/timer/). In this study, we analysed the relationship between PRKCSH expression and the abundance of infiltrating immune cells (including $CD4^+$ T cells, $CD8^+$ T cells, B cells, neutrophils, dendritic cells, and macrophages) based on the expression of specific marker genes for each cancer. The tumour-infiltrating immune cells analysed included T cells, B cells, tumour-associated macrophages, monocytes, M1 and M2 macrophages, natural killer cells, neutrophils, dendritic cells, T helper cells, T helper 17 cells, follicular helper T cells, exhausted T cells, and regulatory T cells. The GEPIA database (http://gepia.cancer-pku.cn/index. html) was used to analyse RNA-seq data from 8,587 normal and 9,736 tumour tissue samples from the TCGA and GTEx projects [26]. We also used the GEPIA website to generate survival curves and determine OS and DFS rates. We identified correlations in the expression patterns of particular genes in 33 different types of cancer to confirm the results of the TIMER analysis. We used the open-access cBioPortal website resource (www.cbioportal.org) to investigate multidimensional cancer genomic datasets [19]. We selected the LUAD (TCGA, provisional) and lung squamous cell carcinoma (TCGA, provisional) datasets to analyse alterations in the PRKCSH and STAT6 genes in NSCLC. The genomic profiles included mutations, putative copy number alterations, and mRNA expression levels (RNA Seq V2 RSEM with z scores = ± 2). We also used the Human Protein Atlas (HPA, http://www.proteinatlas.org) database, which contains transcriptomic, proteomic, and immunohistochemical expression data. This database includes tissue, cell, and

pathology atlases. We obtained the fragments per kilobase of exons per million fragments mapped values and protein expression patterns for PRKCSH and STAT6 in NSCLC patients from the HPA database. The data are presented as immunohistochemical staining images and mRNA expression levels.

Cell lines, antibodies, treatments, small-interfering RNAs, and transfection reagents

Human A549 and HepG2 cells were purchased from the American Type Culture Collection (ATCC, Manassas, VA, USA) and cultured in Dulbecco's modified Eagle's medium supplemented with 10% foetal bovine serum, 100 μg/mL streptomycin, and 100 U/mL penicillin in a humidified 5% CO_2 atmosphere at 37°C, in accordance with the manufacturer's instructions. GAPDH, STAT6, p-STAT6, p53, p-ATM, p-DNApkcs, p-ATR, KAP1, p-CHK1, p-CHK2, p-RPA2, RPA2, and phosphohistone H3 were purchased either from Santa Cruz Biotechnology (Santa Cruz, CA, USA) or Cell Signaling Technology (Danvers, MA, USA). Nano ZnO was purchased from Shanghai Macklin Biochemical Co., Ltd. (CAS: 1314-13-2; Shanghai, China). The cells were treated with 30 μg/mL Nano ZnO at room temperature. This dose was selected based on our pilot dose–response experiments. The methods used to knock down the expression of PRKCSH are described in our previous study [14]. Briefly, small-interfering RNA duplexes were designed and synthesized by Shanghai GenePharma (Shanghai, China) and transfected into the cells using Lipofectamine 2000 (Thermo Fisher Scientific, Waltham, MA, USA) in accordance with the manufacturer's instructions. Scrambled small-interfering RNA was used as a negative control. At 48 h after transfection, the cells were collected for further analyses.

Nano ZnO preparation

The Nano ZnO used in this study was purchased from Shanghai Macklin Biochemical Co., Ltd. The NO size and zeta potential of Nano ZnO were observed using a Malvern Zetasizer Nano ZS90. The photographs of Nano ZnO were obtained by transmission electron microscopy (TEM). All the characteristics of Nano ZnO were determined by the Shiyanjia Laboratory (www.shiyanjia.com). The mean diameter of Nano ZnO at a power of 20 nm was determined by TEM, and the mean hydrodynamic size was 351.2 nm, as determined by dynamic light scattering (DLS) using a Malvern Zetasizer Nano ZS90. Nano ZnO was dispersed in physiological saline, ultrasonicated for 10 min in an FS30 ultrasonic cleaner (Fisher

Scientific, Pittsburgh, PA), and vortexed thoroughly prior to each experiment.

Cell cycle analyses and G2/M arrest assays

For the cell culture experiments, cells were seeded in 35-mm culture dishes at a density of 70–80% per dish. After the cells were harvested, they were treated with RNase A and incubated at 37°C for 30 min. Then, the cells were stained with propidium iodide solution, and the cell cycle distribution was analysed using flow cytometry (A00-1-1102; Beckman Coulter, Inc., Suzhou, China), as described in our previous study [58]. To evaluate G2/M arrest in PRKCSH-WT and PRKCSH-KD cells after Nano ZnO treatment, mitotic cells were counted using flow cytometry (A00-1-1102; Beckman Coulter, Inc.). Cells were incubated with or without Nano ZnO and harvested at various time points (0, 2, 4, 6, 8, or 12 h after treatment). First, phosphate-buffered saline was added to resuspend the cells. Next, the cells were centrifuged at 2,000 rpm, and 0.25% Triton X-100 was added to rupture the cell membranes. After the addition of 40 μL of 1% bovine serum albumin containing anti-Ser10-phosphorylated histone H3 antibody, the cells were incubated for 50 min at room temperature. Next, 80 μL of 1% bovine serum albumin containing a fluorescein isothiocyanate-tagged secondary antibody was added. The cells were then incubated for 30 min and stained with 20 μg/mL propidium iodide solution for 10–30 min at room temperature. Finally, the mitotic cells were counted using flow cytometry. Two-dimensional dot plots were generated using ModFit LT software (ver. 3.0; Verity Software House, Inc., Topsham, ME, USA).

Western blotting

Protein extraction and western blotting were performed as described previously [20]. Images were captured and assessed using the ChemiDoc XRS+ system (Bio-Rad, Hercules, CA, USA). Protein expression was quantified using Image Lab software (ver. 6.1; Bio-Rad). At least three independent replicates were analysed per sample.

Dual-luciferase reporter assays

Predictive and dual-luciferase reporter assays were performed to confirm the interaction between STAT6 and p53. We used data from the National Center for Biotechnology Information to identify the promoter sequence of p53, including approximately 1,000 bases upstream (https://www.ncbi.nlm.nih.gov/). Next, we used the ALGGEN website (http://alggen.lsi.upc.es/) to predict potential binding sites for STAT6 in the p53 promoter

sequence. The p53 promoter region was amplified from genomic DNA extracted from A549 cells and cloned into the pGL3 luciferase vector. The 3′-untranslated region of p53 was also amplified from genomic DNA and cloned into the pGL3 luciferase vector. Briefly, the steps for the construction of pGL3 recombinants with a truncated sequence of the p53 promoter region are described below. First, we designed specific PCR primer sets for the amplification of the p53 promoter region using Primer Premier 5.0 after retrieving the nucleotide sequence from the Ensembl genome browser. Then, we amplified 5 truncated target fragments, and the longest target fragment was -1000 bp---+126. This longest fragment was used as a template to amplify the other truncated fragments. NheI and XhoI restriction endonuclease sites were introduced into the 5’ and 3' ends of the primers, respectively (Table S2). The purified target sequences were cloned into the pGL3 vector. The STAT6 binding site in the p53 promoter was modified using site-directed mutagenesis (Quik-Change Site-Directed Mutagenesis kit; Agilent Technologies, Santa Clara, CA, USA). Lipofectamine 2000 reagent was then used to transiently transfect the reporter plasmids into A549 cells. The reporter assay was conducted 48 h after transfection using the dual-luciferase assay system, as described previously [58-60]. Three biological replicates were used for each experiment, and each experiment was repeated at least three times.

CoIP assays

For the CoIP assays, PRKCSH-WT cells and PRKCSH-KD cells were incubated with or without Nano ZnO. Next, the cells were washed, harvested, and lysed in phosphate-buffered saline containing 50 nM Tris-base, 1 mM ethylenediaminetetraacetic acid, 1% NP-40, and 1× protease inhibitor cocktail. The lysates were centrifuged, and the supernatants were collected for CoIP assays using the Pierce Classic IP kit (Thermo Fisher Scientific). A STAT6 antibody was used to generate immunocomplexes with p53 and ATM. These immunocomplexes were separated using 8% sodium dodecyl sulfate–polyacrylamide gel electrophoresis, washed, and eluted. Protein interactions were detected by western blotting, as described previously [61].

Immunofluorescence staining and confocal laser microscopy

The localization of the STAT6 and p53 proteins after Nano ZnO treatment was visualized by immunofluorescence staining and confocal laser microscopy. The nuclei of control A549 cells stained with 4',6-diamidino-2-phenylindole were blue. At 4 h after

transfection, the cells were treated with Nano ZnO and 0.25% Triton X-100. After incubation with the secondary antibody, all experimental steps were performed in the dark. Samples incubated with 5% bovine serum albumin instead of the primary antibody were used as negative controls. The samples were visualized using an LSM 510 confocal laser scanning microscope (Carl Zeiss, Oberkochen, Germany).

Statistical analyses

All data are reported as the means ± standard deviation, and a p value < 0.05 was considered statistically significant (Student's t test). A fold change ≥ 2.0 and p value < 0.05 indicated differential mRNA expression. Unpaired numerical data were compared using the unpaired t test *(*two groups) or analysis of variance (more than two groups). Statistical analyses were performed using SPSS for Windows software (ver. 22.0; SPSS Inc., Chicago, IL, USA).

Ethical Approval and Consent to participate

N/A

Consent for publication

N/A

Availability of supporting data

N/A

Competing interests

The authors declare no competing financial interests.

Acknowledgments

This study was supported by grants from the National Natural Science Foundation of China (Grant Nos. 82073486, U1803124), Scientific research project of Hunan Health Committee (202112010058), Natural Science Foundation of Hunan Province (2019JJ40397), and Scientific research project of Hunan Provincial Health Commission (202112010058), the Graduate Research Innovation Program of Central South University (No.2021zzts0325, 2021zzts0966, 2021zzts0970).

Authors' contributions

Ruixue Huang: Conceptualization, Methodology, Formal analysis, Investigation, critically revised final manuscript, Funding acquisition; RD L, ML Z: Investigation, cell experiments,

Formal analysis, wrote the draft of study; C Q, Y W, SS Z and JH L: Investigation, cell experiments, Formal analysis, All the authors read and approved the manuscript.

Reference

1. Hirsch FR, Scagliotti GV, Mulshine JL, Kwon R, Curran WJ, Jr., Wu YL, Paz-Ares L: **Lung cancer: current therapies and new targeted treatments**. *Lancet* 2017, **389**(10066):299-311.
2. Landman A: **2021 World Conference on Lung Cancer**. *Lancet Oncol* 2021, **22**(10):e429.
3. Burki TK: **Developments in lung cancer biology in never-smokers**. *Lancet Oncol* 2021, **22**(10):1363.
4. Wang J, Wang H, Wang H, He S, Li R, Deng Z, Liu X, Wang F: **Nonviolent Self-Catabolic DNAzyme Nanosponges for Smart Anticancer Drug Delivery**. *ACS Nano* 2019, **13**(5):5852-5863.
5. Thomas S, Gunasangkaran G, Arumugam VA, Muthukrishnan S: **Synthesis and Characterization of Zinc Oxide Nanoparticles of Solanum nigrum and Its Anticancer Activity via the Induction of Apoptosis in Cervical Cancer**. *Biol Trace Elem Res* 2021.
6. Goldstraw P, Chansky K, Crowley J, Rami-Porta R, Asamura H, Eberhardt WE, Nicholson AG, Groome P, Mitchell A, Bolejack V *et al*: **The IASLC Lung Cancer Staging Project: Proposals for Revision of the TNM Stage Groupings in the Forthcoming (Eighth) Edition of the TNM Classification for Lung Cancer**. *J Thorac Oncol* 2016, **11**(1):39-51.
7. Senan S, Brade A, Wang LH, Vansteenkiste J, Dakhil S, Biesma B, Martinez Aguillo M, Aerts J, Govindan R, Rubio-Viqueira B *et al*: **PROCLAIM: Randomized Phase III Trial of Pemetrexed-Cisplatin or Etoposide-Cisplatin Plus Thoracic Radiation Therapy Followed by Consolidation Chemotherapy in Locally Advanced Nonsquamous Non-Small-Cell Lung Cancer**. *J Clin Oncol* 2016, **34**(9):953-962.
8. Forde PM, Kelly RJ, Brahmer JR: **New strategies in lung cancer: translating immunotherapy into clinical practice**. *Clin Cancer Res* 2014, **20**(5):1067-1073.
9. Gao H, Wang Y, Wegierski T, Skouloudaki K, Putz M, Fu X, Engel C, Boehlke C, Peng H, Kuehn EW *et al*: **PRKCSH/80K-H, the protein mutated in polycystic liver disease, protects polycystin-2/TRPP2 against HERP-mediated degradation**. *Hum Mol Genet* 2010, **19**(1):16-24.
10. Shin GC, Moon SU, Kang HS, Choi HS, Han HD, Kim KH: **PRKCSH contributes to tumorigenesis by selective boosting of IRE1 signaling pathway**. *Nat Commun* 2019, **10**(1):3185.
11. Lee HH, Lim CA, Cheong YT, Singh M, Gam LH: **Comparison of protein expression profiles of different stages of lymph nodes metastasis in breast cancer**. *Int J Biol Sci* 2012, **8**(3):353-362.
12. Sudo M, Mori S, Madan V, Yang H, Leong G, Koeffler HP: **Short-hairpin RNA library: identification of therapeutic partners for gefitinib-resistant non-small cell lung cancer**. *Oncotarget* 2015, **6**(2):814-824.
13. Khaodee W, Inboot N, Udomsom S, Kumsaiyai W, Cressey R: **Glucosidase II beta subunit (GluIIbeta) plays a role in autophagy and apoptosis regulation in lung carcinoma cells in a p53-dependent manner**. *Cell Oncol (Dordr)* 2017, **40**(6):579-591.
14. Huang R, Liu X, Li H, Ning H, Zhou PK: **PRKCSH Alternative Splicing Involves in Silica-Induced Expression of Epithelial-Mesenchymal Transition Markers and Cell**

Proliferation. *Dose Response* 2020, **18**(2):1559325820923825.

15. Bai DP, Zhang XF, Zhang GL, Huang YF, Gurunathan S: **Zinc oxide nanoparticles induce apoptosis and autophagy in human ovarian cancer cells**. *Int J Nanomedicine* 2017, **12**:6521-6535.
16. Hanley C, Layne J, Punnoose A, Reddy KM, Coombs I, Coombs A, Feris K, Wingett D: **Preferential killing of cancer cells and activated human T cells using ZnO nanoparticles**. *Nanotechnology* 2008, **19**(29):295103.
17. Chen R, Huo L, Shi X, Bai R, Zhang Z, Zhao Y, Chang Y, Chen C: **Endoplasmic reticulum stress induced by zinc oxide nanoparticles is an earlier biomarker for nanotoxicological evaluation**. *ACS Nano* 2014, **8**(3):2562-2574.
18. Sharma A, Gorey B, Casey A: **In vitro comparative cytotoxicity study of aminated polystyrene, zinc oxide and silver nanoparticles on a cervical cancer cell line**. *Drug Chem Toxicol* 2019, **42**(1):9-23.
19. Bisht G, Rayamajhi S: **ZnO Nanoparticles: A Promising Anticancer Agent**. *Nanobiomedicine (Rij)* 2016, **3**:9.
20. Ju Z, Shao J, Zhou M, Jin J, Pan H, Ding P, Huang R: **Transcriptomic and metabolomic profiling reveal the p53-dependent benzeneacetic acid attenuation of silica-induced epithelial-mesenchymal transition in human bronchial epithelial cells**. *Cell Biosci* 2021, **11**(1):30.
21. Ye BL, Zheng R, Ruan XJ, Zheng ZH, Cai HJ: **Chitosan-coated doxorubicin nano-particles drug delivery system inhibits cell growth of liver cancer via p53/PRC1 pathway**. *Biochem Biophys Res Commun* 2018, **495**(1):414-420.
22. Anwar MM, Abd El-Karim SS, Mahmoud AH, Amr AEE, Al-Omar MA: **A Comparative Study of the Anticancer Activity and PARP-1 Inhibiting Effect of Benzofuran-Pyrazole Scaffold and Its Nano-Sized Particles in Human Breast Cancer Cells**. *Molecules* 2019, **24**(13).
23. Yin L, Yu X: **Arsenic-induced apoptosis in the p53-proficient and p53-deficient cells through differential modulation of NFkB pathway**. *Food Chem Toxicol* 2018, **118**:849-860.
24. Randrian V, Desette A, Emambux S, Derangere V, Roussille P, Frouin E, Godet J, Karayan-Tapon L, Ghiringhelli F, Tougeron D: **New Artificial Intelligence Score and Immune Infiltrates as Prognostic Factors in Colorectal Cancer With Brain Metastases**. *Front Immunol* 2021, **12**:750407.
25. Wang YQ, Liu X, Xu C, Jiang W, Xu SY, Zhang Y, Liang YL, Li JY, Li Q, Chen YP *et al*: **Spatial heterogeneity of immune infiltration predicts the prognosis of nasopharyngeal carcinoma patients**. *Oncoimmunology* 2021, **10**(1):1976439.
26. Li T, Fu J, Zeng Z, Cohen D, Li J, Chen Q, Li B, Liu XS: **TIMER2.0 for analysis of tumor-infiltrating immune cells**. *Nucleic Acids Res* 2020, **48**(W1):W509-W514.
27. Li T, Fan J, Wang B, Traugh N, Chen Q, Liu JS, Li B, Liu XS: **TIMER: A Web Server for Comprehensive Analysis of Tumor-Infiltrating Immune Cells**. *Cancer Res* 2017, **77**(21):e108-e110.
28. Meng X, Gao JZ, Gomendoza SMT, Li JW, Yang S: **Recent Advances of WEE1 Inhibitors and Statins in Cancers With p53 Mutations**. *Front Med (Lausanne)* 2021, **8**:737951.
29. Cao H, Zhang J, Liu H, Wan L, Zhang H, Huang Q, Xu E, Lai M: **IL-13/STAT6 signaling plays a critical role in the epithelial-mesenchymal transition of colorectal cancer cells**.

Oncotarget 2016, **7**(38):61183-61198.

30. Lodovichi S, Belle F, Cervelli T, Lorenzoni A, Maresca L, Cozzani C, Caligo MA, Galli A: **Effect of BRCA1 missense variants on gene reversion in DNA double-strand break repair mutants and cell cycle-arrested cells of Saccharomyces cerevisiae**. *Mutagenesis* 2020, **35**(2):189-195.
31. Schinelli S, Frattini P, Cucchi ML, Peroni AE, Santagostino G: **Determination of vanillylmandelic acid in plasma by high-performance liquid chromatography with electrochemical detection**. *J Chromatogr* 1988, **431**(1):150-155.
32. Huang R, Zhou PK: **DNA damage repair: historical perspectives, mechanistic pathways and clinical translation for targeted cancer therapy**. *Signal Transduct Target Ther* 2021, **6**(1):254.
33. Liu H, Zhao H: **Prognosis related miRNAs, DNA methylation, and epigenetic interactions in lung adenocarcinoma**. *Neoplasma* 2019, **66**(3):487-493.
34. Chen FC, Huang CM, Yu XW, Chen YY: **Effect of nano zinc oxide on proliferation and toxicity of human gingival cells**. *Hum Exp Toxicol* 2022, **41**:9603271221080236.
35. Farcal L, Torres Andon F, Di Cristo L, Rotoli BM, Bussolati O, Bergamaschi E, Mech A, Hartmann NB, Rasmussen K, Riego-Sintes J *et al*: **Comprehensive In Vitro Toxicity Testing of a Panel of Representative Oxide Nanomaterials: First Steps towards an Intelligent Testing Strategy**. *PLoS One* 2015, **10**(5):e0127174.
36. Jiang F, Liang M, Huang X, Shi W, Wang Y: **High expression of PIMREG predicts poor survival outcomes and is correlated with immune infiltrates in lung adenocarcinoma**. *PeerJ* 2021, **9**:e11697.
37. Wang W, Ren S, Wang Z, Zhang C, Huang J: **Increased expression of TTC21A in lung adenocarcinoma infers favorable prognosis and high immune infiltrating level**. *Int Immunopharmacol* 2020, **78**:106077.
38. Wang SS, Liu W, Ly D, Xu H, Qu L, Zhang L: **Tumor-infiltrating B cells: their role and application in anti-tumor immunity in lung cancer**. *Cell Mol Immunol* 2019, **16**(1):6-18.
39. Wang Z, Zhang M, Wu Y, Yu Y, Zheng Q, Li J: **CKS2 Overexpression Correlates with Prognosis and Immune Cell Infiltration in Lung Adenocarcinoma: A Comprehensive Study based on Bioinformatics and Experiments**. *J Cancer* 2021, **12**(23):6964-6978.
40. Liu X, Yin M, Dong J, Mao G, Min W, Kuang Z, Yang P, Liu L, Zhang N, Deng H: **Tubeimoside-1 induces TFEB-dependent lysosomal degradation of PD-L1 and promotes antitumor immunity by targeting mTOR**. *Acta Pharm Sin B* 2021, **11**(10):3134-3149.
41. Li Q, Yao L, Lin Z, Li F, Xie D, Li C, Zhan W, Lin W, Huang L, Wu S *et al*: **Identification of Prognostic Model Based on Immune-Related LncRNAs in Stage I-III Non-Small Cell Lung Cancer**. *Front Oncol* 2021, **11**:706616.
42. Hebenstreit D, Wirnsberger G, Horejs-Hoeck J, Duschl A: **Signaling mechanisms, interaction partners, and target genes of STAT6**. *Cytokine Growth Factor Rev* 2006, **17**(3):173-188.
43. Son DJ, Jung YY, Park MH, Lee HL, Song MJ, Yoo HS, Hwang DY, Han SB, Hong JT: **Activated Natural Killer Cells Mediate the Suppressive Effect of Interleukin-4 on Tumor Development via STAT6 Activation in an Atopic Condition Melanoma Model**. *Neoplasia* 2017, **19**(7):537-548.
44. Wang L, Yu S, Yin Y, Hao Y: **STAT6 correlates with response to immune checkpoint**

blockade therapy and predicts worse survival in thyroid cancer. *Biomark Med* 2020, **14**(11):955-967.

45. Fu C, Jiang L, Hao S, Liu Z, Ding S, Zhang W, Yang X, Li S: **Activation of the IL-4/STAT6 Signaling Pathway Promotes Lung Cancer Progression by Increasing M2 Myeloid Cells**. *Front Immunol* 2019, **10**:2638.
46. Geskin LJ, Viragova S, Stolz DB, Fuschiotti P: **Interleukin-13 is overexpressed in cutaneous T-cell lymphoma cells and regulates their proliferation**. *Blood* 2015, **125**(18):2798-2805.
47. Ji W, Liu Y, Xu B, Mei J, Cheng C, Xiao Y, Yang K, Huang W, Jiao J, Liu H *et al*: **Bioinformatics Analysis of Expression Profiles and Prognostic Values of the Signal Transducer and Activator of Transcription Family Genes in Glioma**. *Front Genet* 2021, **12**:625234.
48. Yang X, Shao H, Liu W, Gu W, Shu X, Mo Y, Chen X, Zhang Q, Jiang M: **Endoplasmic reticulum stress and oxidative stress are involved in ZnO nanoparticle-induced hepatotoxicity**. *Toxicol Lett* 2015, **234**(1):40-49.
49. Yang R, Wu R, Mei J, Hu FR, Lei CJ: **Zinc oxide nanoparticles promotes liver cancer cell apoptosis through inducing autophagy and promoting p53**. *Eur Rev Med Pharmacol Sci* 2021, **25**(3):1557-1563.
50. Toprani SM, Bitounis D, Huang Q, Oliveira N, Ng KW, Tay CY, Nagel ZD, Demokritou P: **High-Throughput Screening Platform for Nanoparticle-Mediated Alterations of DNA Repair Capacity**. *ACS Nano* 2021, **15**(3):4728-4746.
51. Murali M, Anandan S, Ansari MA, Alzohairy MA, Alomary MN, Asiri SMM, Almatroudi A, Thriveni MC, Singh SB, Gowtham HG *et al*: **Genotoxic and Cytotoxic Properties of Zinc Oxide Nanoparticles Phyto-Fabricated from the Obscure Morning Glory Plant Ipomoea obscura (L.) Ker Gawl**. *Molecules* 2021, **26**(4).
52. Ebrahimi M, Babaei E, Neri F, Feizi MAH: **Anti-proliferative and apoptotic effect of gemini curcumin in p53-wild type and p53-mutant colorectal cancer cell lines**. *Int J Pharm* 2021, **601**:120592.
53. Liang X, Zhang D, Liu W, Yan Y, Zhou F, Wu W, Yan Z: **Reactive oxygen species trigger NF-kappaB-mediated NLRP3 inflammasome activation induced by zinc oxide nanoparticles in A549 cells**. *Toxicol Ind Health* 2017, **33**(10):737-745.
54. Wang C, Hu X, Gao Y, Ji Y: **ZnO Nanoparticles Treatment Induces Apoptosis by Increasing Intracellular ROS Levels in LTEP-a-2 Cells**. *Biomed Res Int* 2015, **2015**:423287.
55. Yu JE, Yeo IJ, Son DJ, Yun J, Han SB, Hong JT: **Anti-Chi3L1 antibody suppresses lung tumor growth and metastasis through inhibition of M2 polarization**. *Mol Oncol* 2021.
56. Zheng Z, Li YN, Jia S, Zhu M, Cao L, Tao M, Jiang J, Zhan S, Chen Y, Gao PJ *et al*: **Lung mesenchymal stromal cells influenced by Th2 cytokines mobilize neutrophils and facilitate metastasis by producing complement C3**. *Nat Commun* 2021, **12**(1):6202.
57. Nonaka H, Kandori S, Nitta S, Shiga M, Nagumo Y, Kimura T, Kawahara T, Negoro H, Hoshi A, Kojima T *et al*: **Case Report: Molecular Characterization of Aggressive Malignant Retroperitoneal Solitary Fibrous Tumor: A Case Study**. *Front Oncol* 2021, **11**:736969.
58. Dai X, Huang R, Hu S, Zhou Y, Sun X, Gui P, Yu Z, Zhou P: **A novel miR-0308-3p revealed**

by miRNA-seq of HBV-positive hepatocellular carcinoma suppresses cell proliferation and promotes G1/S arrest by targeting double CDK6/Cyclin D1 genes. *Cell Biosci* 2020, **10**:24.

59. Mo LJ, Song M, Huang QH, Guan H, Liu XD, Xie DF, Huang B, Huang RX, Zhou PK: **Exosome-packaged miR-1246 contributes to bystander DNA damage by targeting LIG4**. *Br J Cancer* 2018, **119**(4):492-502.
60. Huang R, Bai C, Liu X, Zhou Y, Hu S, Li D, Xiang J, Chen J, Zhou P: **The p53/RMRP/miR122 signaling loop promotes epithelial-mesenchymal transition during the development of silica-induced lung fibrosis by activating the notch pathway**. *Chemosphere* 2021, **263**:128133.
61. Huang R, Gao S, Han Y, Ning H, Zhou Y, Guan H, Liu X, Yan S, Zhou PK: **BECN1 promotes radiation-induced G2/M arrest through regulation CDK1 activity: a potential role for autophagy in G2/M checkpoint**. *Cell Death Discov* 2020, **6**:70.

Figure legend:

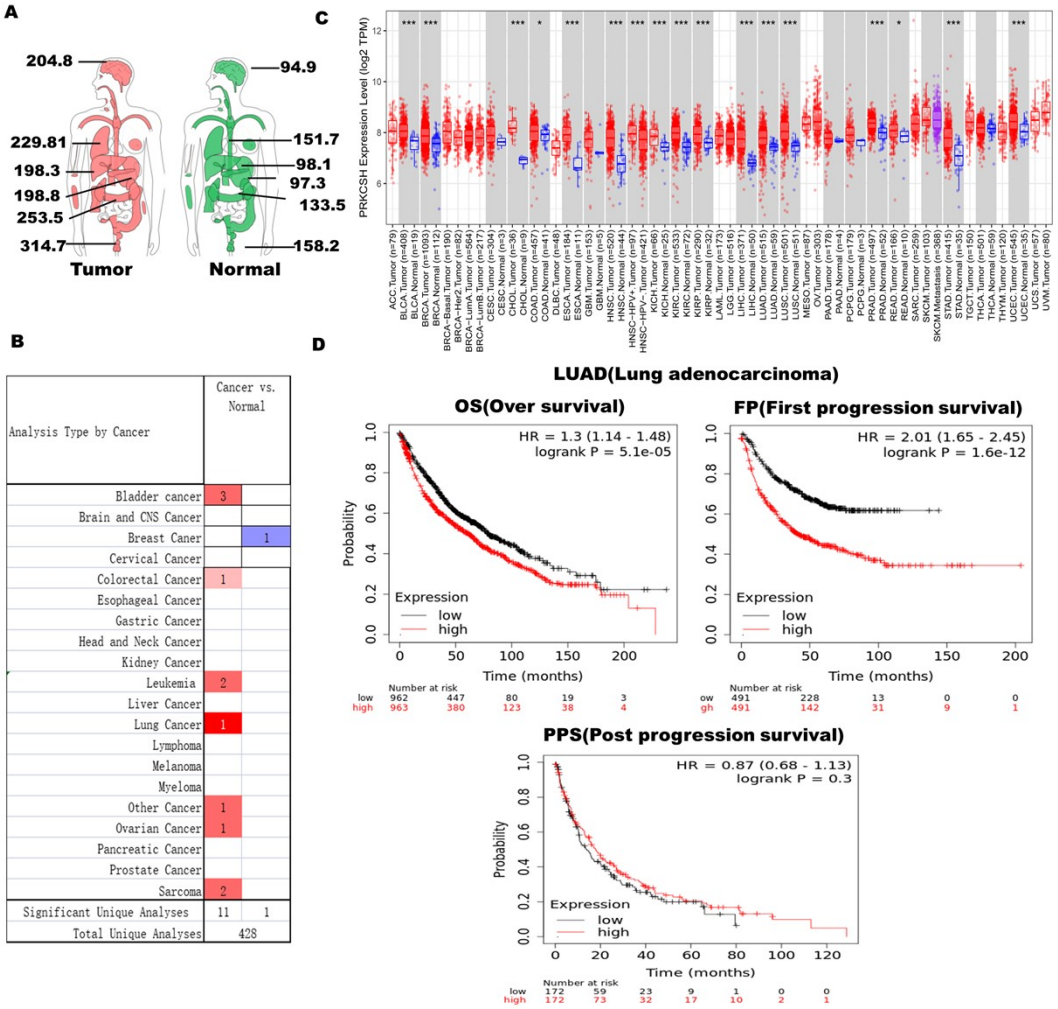

Figure 1. **The level of PRKCSH is increased in various cancer tissues.** (A). Map of human organs in which the expression of PRKCSH mRNA is significantly higher in tumours than in nontumour tissues. Gene expression datasets from The Cancer Genome Atlas (TCGA) database were analysed by using the Gene Expression Profiling Interactive Analysis (GEPIA) web tool. (B). Representative illustration of PRKCSH mRNA expression in cancer tissues and normal tissues. Red indicates a gene rank percentile (%) increase from 1 to 10, while blue indicates a gene rank percentile (%) reduction from 10 to 1. (C). Comparative analysis of PRKCSH expression in various cancers and normal tissues using the TCGA database through the Tumor Immune Estimation Resource (TIMER) online database. (D). Overall survival (OS), first progression survival (FP) and postprogression survival (PPS) in lung adenocarcinoma (LUAD). The data were obtained from TCGA datasets. The significance of the differences between the two categories was determined by a log-rank test. For

comparative analysis between two groups, one-way analysis of variance (ANOVA) was used. Data are represented as the mean ± standard error of the mean (SEM) of four samples. *p< 0.01. ACC: adrenocortical carcinoma; BLCA; bladder urothelial carcinoma; BRCA-Her2: breast invasive carcinoma; CESC: cervical squamous cell carcinoma and endocervical adenocarcinoma; CHOL: cholangiocarcinoma; COAD: colon adenocarcinoma; DLBC: lymphoid neoplasm diffuse large B cell lymphoma; ESCA: oesophageal carcinoma; GBM: glioblastoma multiforme; HNSC: head and neck squamous cell carcinoma; KICH: kidney chromophobe; KIRC: kidney renal clear cell carcinoma; KIRP: kidney renal papillary cell carcinoma; LAML: acute myeloid leukaemia; LGG: brain lower grade glioma; LIHC: liver hepatocellular carcinoma; LUSC: lung squamous cell carcinoma; MESO: mesothelioma; OV: ovarian serous cystadenocarcinoma; PAAD: pancreatic adenocarcinoma; PCPG: pheochromocytoma and paraganglioma; PRAD: prostate adenocarcinoma; READ: rectum adenocarcinoma; SARC: sarcoma; SKCM: skin cutaneous melanoma; STAD: stomach adenocarcinoma; TGCT: testicular germ cell tumour; THCA: thyroid carcinoma; THYM: thymoma; UCEC: uterine corpus endometrial carcinoma; UVM: uterine carcinosarcoma.

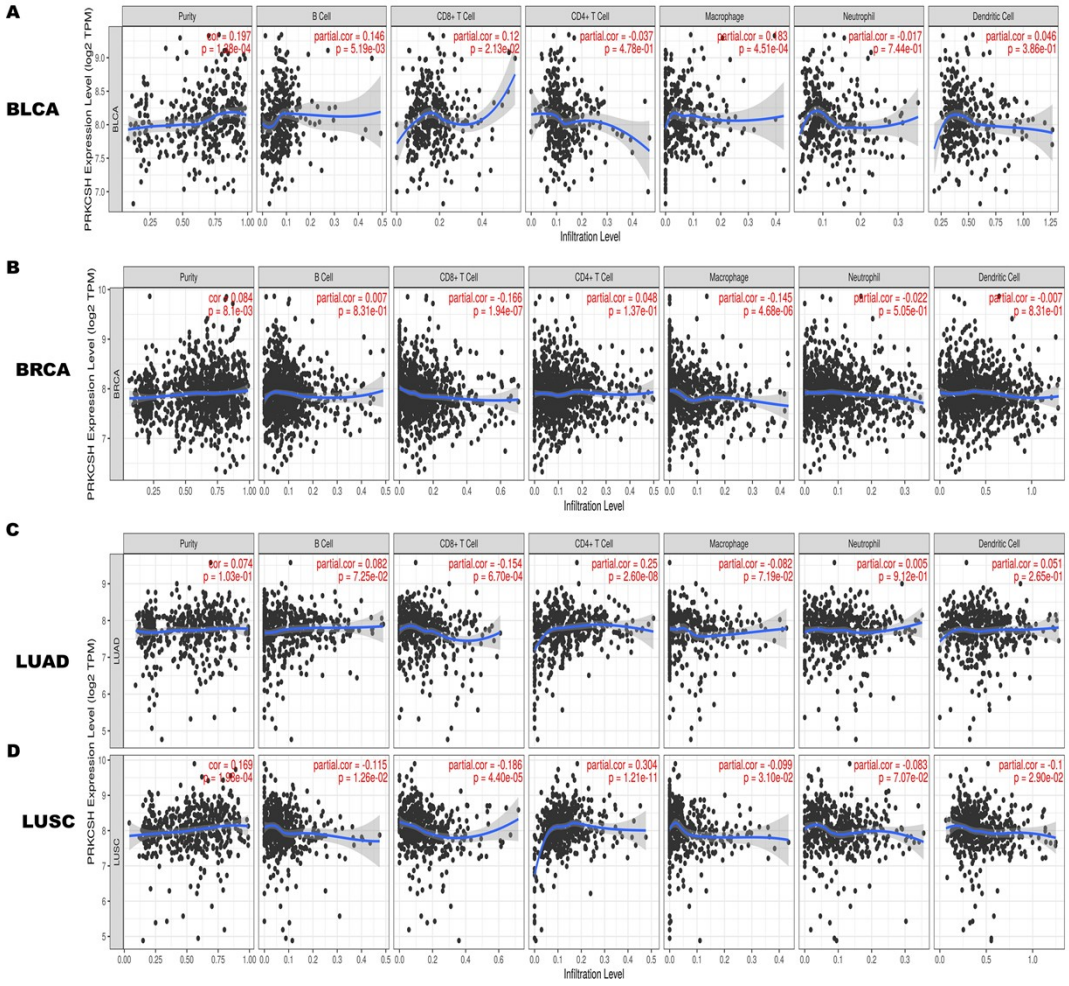

Figure 2. Correlation analysis of PRKCSH expression and infiltration levels of immune cells in BLCA (A), BRCA (B), LUAD (C), and LUSC (D) tissues using the TIMER database. PRKCSH expression in cancer tissues positively correlates with tumour purity and the infiltration levels of B cells, CD8+ T cells, CD4+ T cells, macrophages, neutrophils, and dendritic cells. The scatterplots will be generated and displayed after inputs are submitted successfully, showing the purity-corrected partial Spearman's rho value and statistical significance. The gene expression levels against tumour purity are always displayed in the left-most panel.

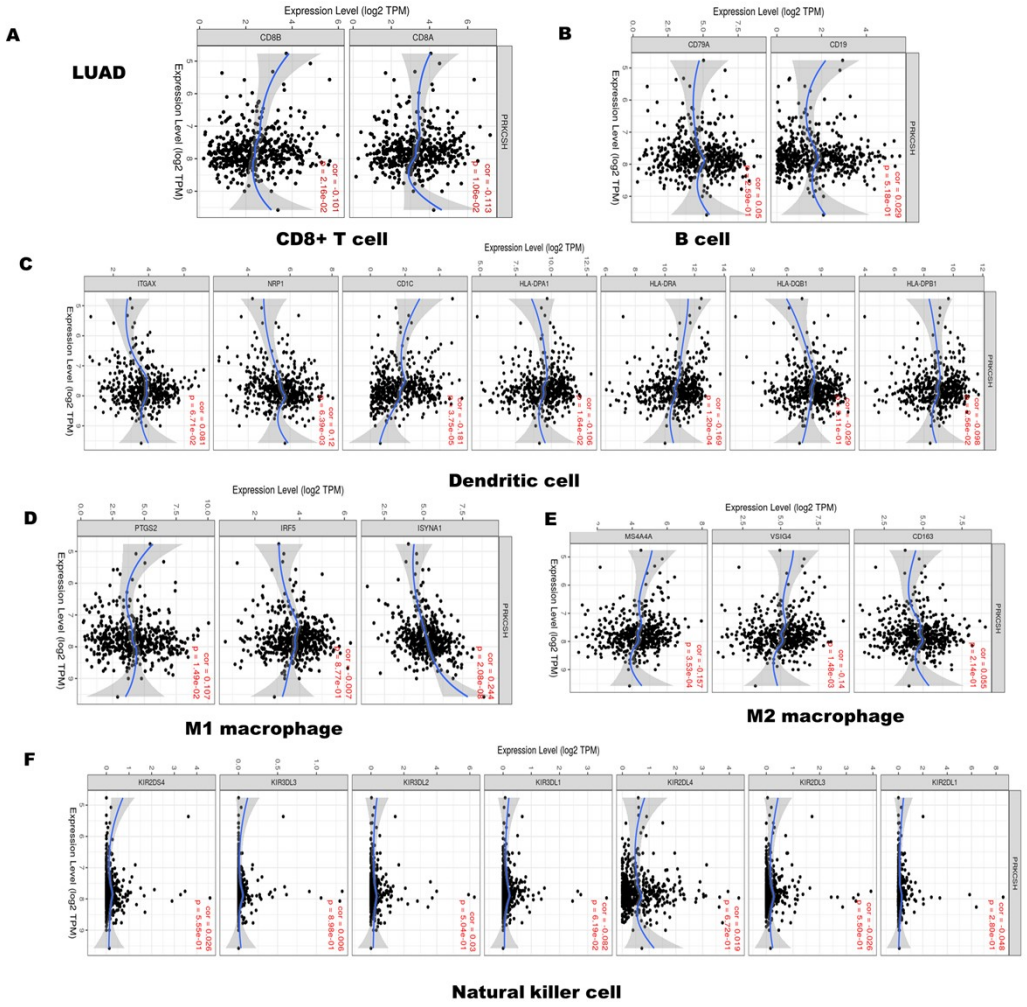

Figure 3. Correlation analysis of PRKCSH expression and infiltration levels of immune cells in LUAD tissues using the GEPIA database. PRKCSH expression in cancer tissues positively correlates with tumour purity and the infiltration levels of CD8+ T cells (A), B cells (B), dendritic cells (C), M1 macrophages (D), M2 macrophages (E), and natural killer cells (F). Scatterplots will be generated and displayed after inputs are submitted successfully, showing the purity-corrected partial Spearman's rho value and statistical significance. The gene expression levels against tumour purity are always displayed in the left-most panel.

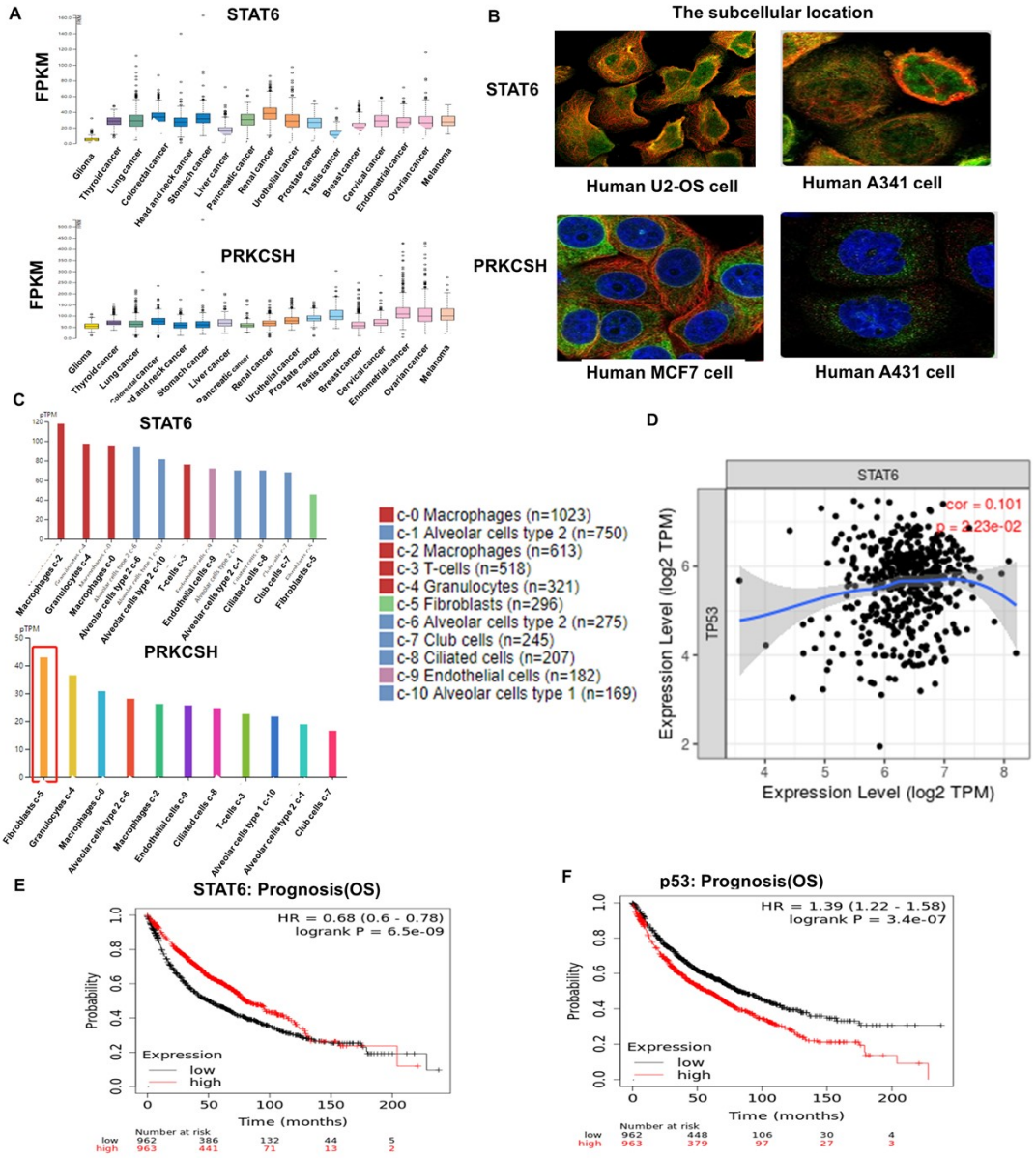

Figure 4. Distributions of STAT6 and PRKCSH. (A). The expression levels of STAT6 and PRKCSH in various cancer tissues were determined using online TCGA databases, and the analysis was conducted by the online website of https://www.proteinatlas.org/. (B). The subcellular locations of STAT6 and PRKCSH in different cancer cells were determined by the online website of https://www.proteinatlas.org/. (C). The expression levels of STAT6 and PRKCSH in various cell lines were determined using the online website of https://www.proteinatlas.org/. (D). Correlation analysis of PRKCSH expression and p53 levels in immune cells in LUAD tissues using the GEPIA database was conducted by the online website https://www.proteinatlas.org/. (E). Prognostic marker in lung cancer (favourable) of STAT6. (F). Prognostic marker in lung cancer (unfavourable) of p53.

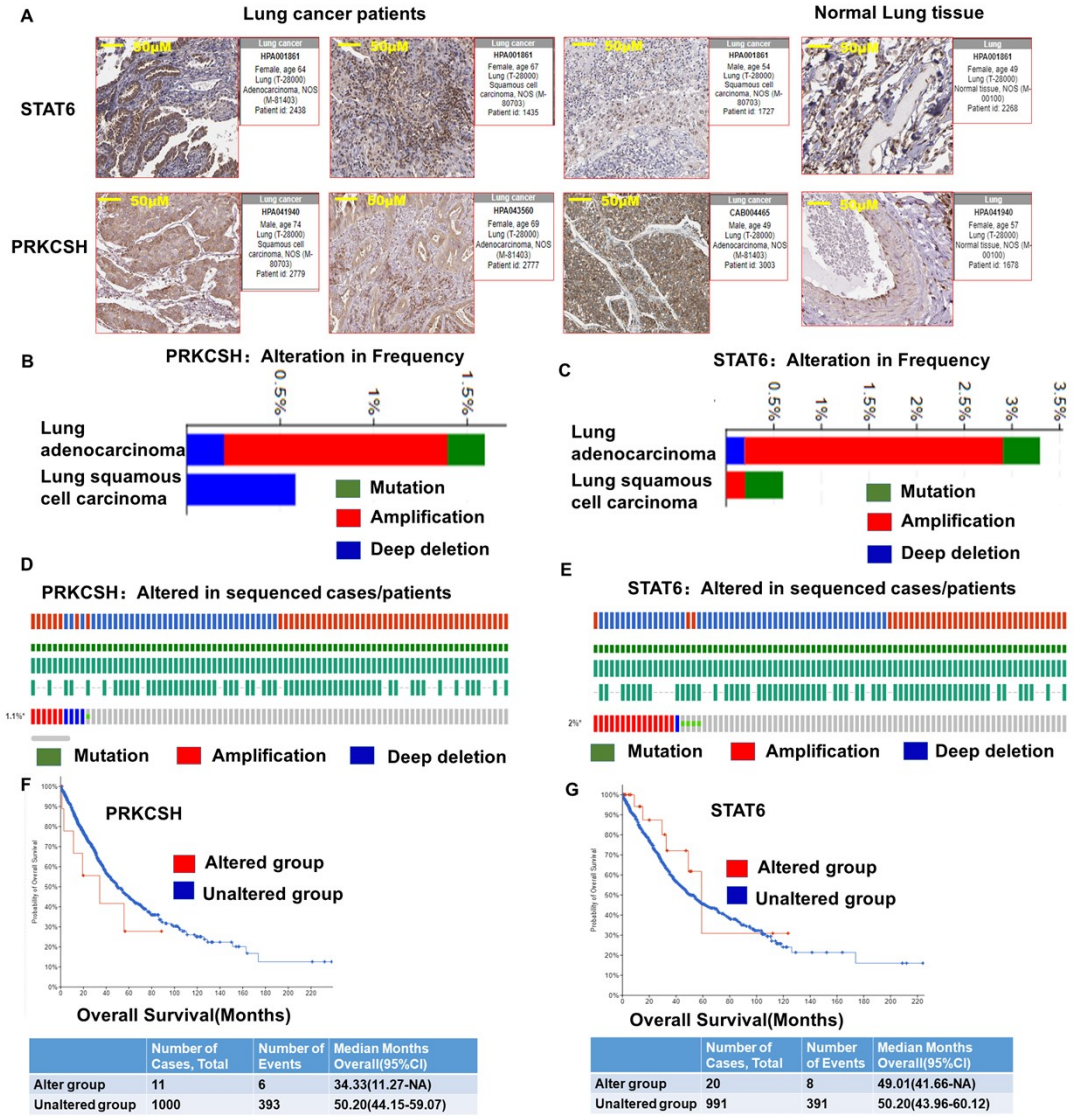

	Number of Cases, Total	Number of Events	Median Months Overall(95%CI)
Alter group	11	6	34.33(11.27-NA)
Unaltered group	1000	393	50.20(44.15-59.07)

	Number of Cases, Total	Number of Events	Median Months Overall(95%CI)
Alter group	20	8	49.01(41.66-NA)
Unaltered group	991	391	50.20(43.96-60.12)

Figure 5. PRKCSH and STAT6 gene expression and mutation analysis in lung cancer. (A). Representative immunohistochemical (IHC) images of STAT6 and PRKCSH expression in lung cancer tissues compared with normal noncancer tissues using TCGA databases on the online website THPA (https://www.proteinatlas.org/ENSG00000130175-PRKCSH/pathology). Scale bar: 50 μM. (B). Alteration in the frequency of PRKCSH gene mutation analysis in lung cancer (http://www.cbioportal.org/) (C). Alteration in the frequency of STAT6 gene mutation analysis in lung cancer (http://www.cbioportal.org/). (D). Altered in sequenced cases/patients of PRKCSH in lung cancer (http://www.cbioportal.org/). (E).

STAT6 was altered in sequenced cases/patients with lung cancer (http://www.cbioportal.org/). (F). OS of PRKCSH in altered lung cancer patients compared with STAT6-unaltered lung cancer patients. (G). OS of STAT6-altered lung cancer patients compared with STAT6-unaltered lung cancer patients.

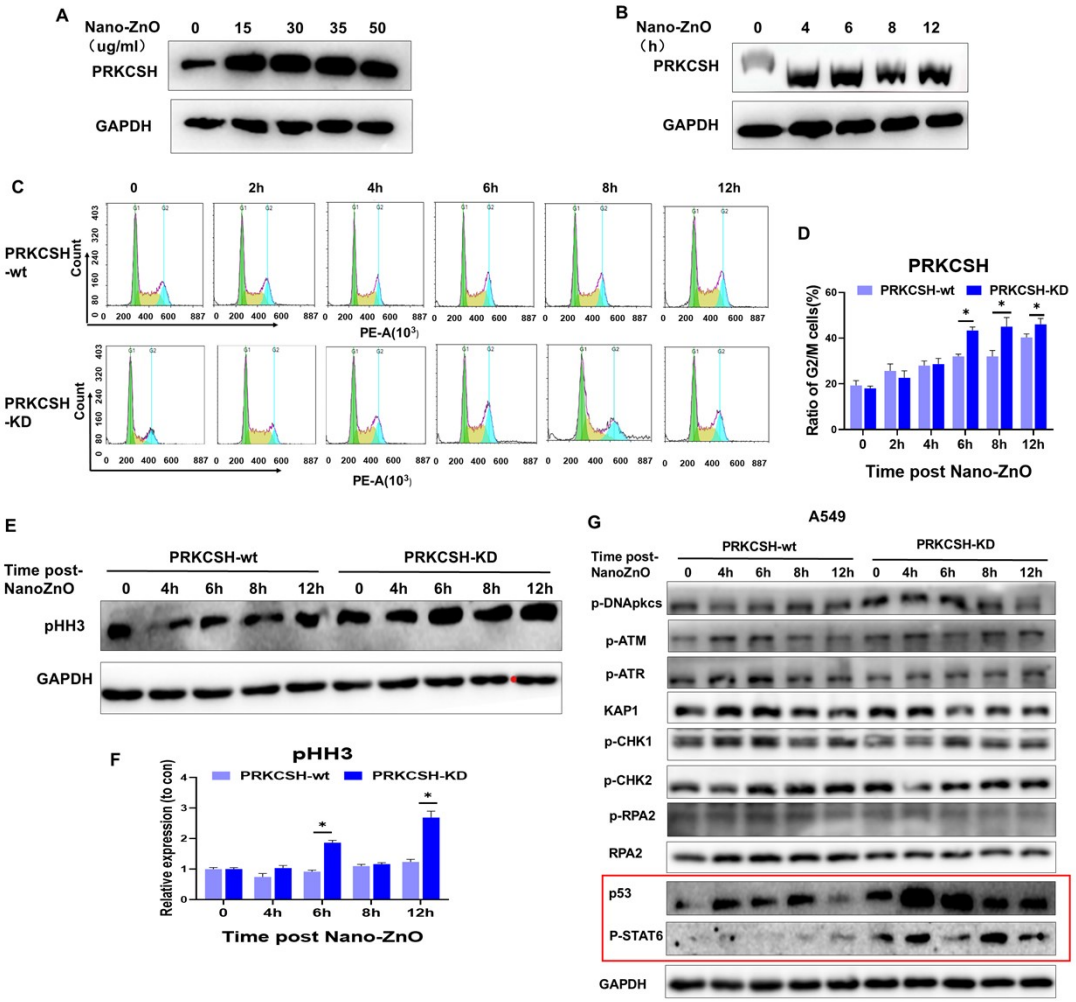

Figure 6. Involvement of PRKCSH in the regulation of Nano-ZnO-induced cell cycle progression arrest. (A). Expression of PRKCSH protein after treatment with various doses of ZnO. (B) Protein expression of PRKCSH after treatment with 30 μg/ml ZnO nanoparticles (Nano ZnO) at the indicated time points. (C). Representative flow cytometry histogram of cell cycle progression in the population of PRKCSH-wild-type (WT) and PRKCSH-knockdown (KD) A549 cancer cells with or without 30 μg/ml ZnO treatment (D). Quantitative measurement of the population of PRKCSH-WT and PRKCSH-KD A549 cancer cells in the G2 and M phases at the indicated times with or without Nano ZnO treatment. (E). pHH3 was detected by Western blotting analysis. GAPDH served as the internal control. (F).

Quantitative measurement of pHH3 expression in RKCSH-WT and PRKCSH-KD A549 cancer cells treated with or without 30 μg/ml Nano ZnO at the indicated time points. (E). Western blotting analysis of G2/M checkpoint-regulating proteins and DNA damage proteins (pDNApkcs, pATM, pATR, KAP1, p-CHK1, p-CHK2, p-RPA2, RPA2, p53, p-STAT6) in the Nano ZnO-treated PRKCSH-wt and PRKCSH-KD A549 cancer cells. GAPDH served as the internal control. GAPDH served as the internal control. The data are presented as the means ± SDs from three independent experiments; *p< 0.05 between different groups.

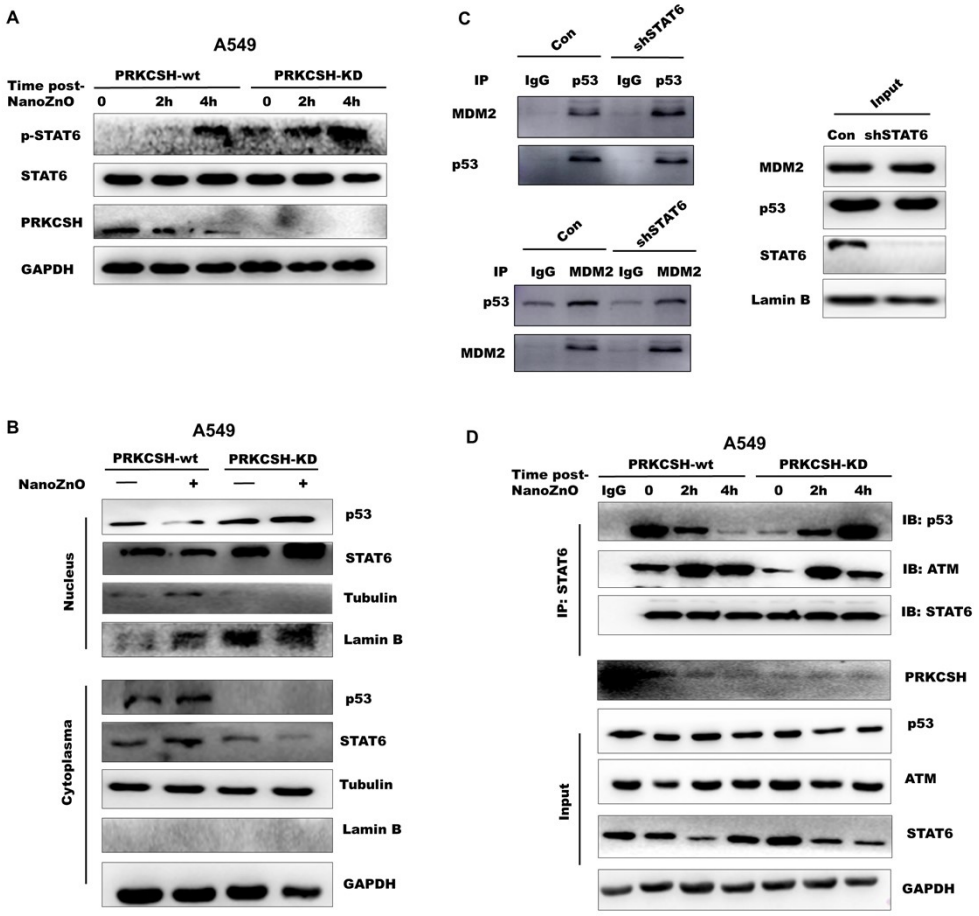

Figure 7. PRKCSH deficiency promotes the translocation of STAT6 from the cytoplasm to the nucleus (A). The levels of phosphorylated STAT6 protein in PRKCSH-KDA549 cells were detected 2 and 4 h after Nano ZnO treatment by western blot analysis. GAPDH served as the internal loading control. (B). The levels of p53 and STAT6 proteins in the cytoplasm and nucleus, respectively, in PRKCSH-WT and PRKCSH-KD A549 cancer cells after Nano ZnO treatment were detected by Western blot analysis. GAPDH served as the internal loading

control. Tubulin and LAMIN A/C proteins were detected as the control cytoplasmic and nuclear proteins, respectively. Exogenous PRKCSH-expressing vectors were transfected into PRKCSH-KO cells for the rescue experiment. (C). KD of STAT6 expression increases the binding of endogenous MDM2 with p53. (D). Effects of PRKCSH deficiency on the protein–protein interactions of the p53-STAT6 complex after Nano ZnO treatment. Cell lysates were collected from PRKCSH-WT and PRKCSH-KDA549 cells at the indicated timepoints after Nano ZnO treatment, and immunoprecipitants were prepared with anti-STAT6 or anti-IgG antibodies. Western blotting analysis was performed using anti-p53 and anti-ATM antibodies. GAPDH was used as the internal loading control.

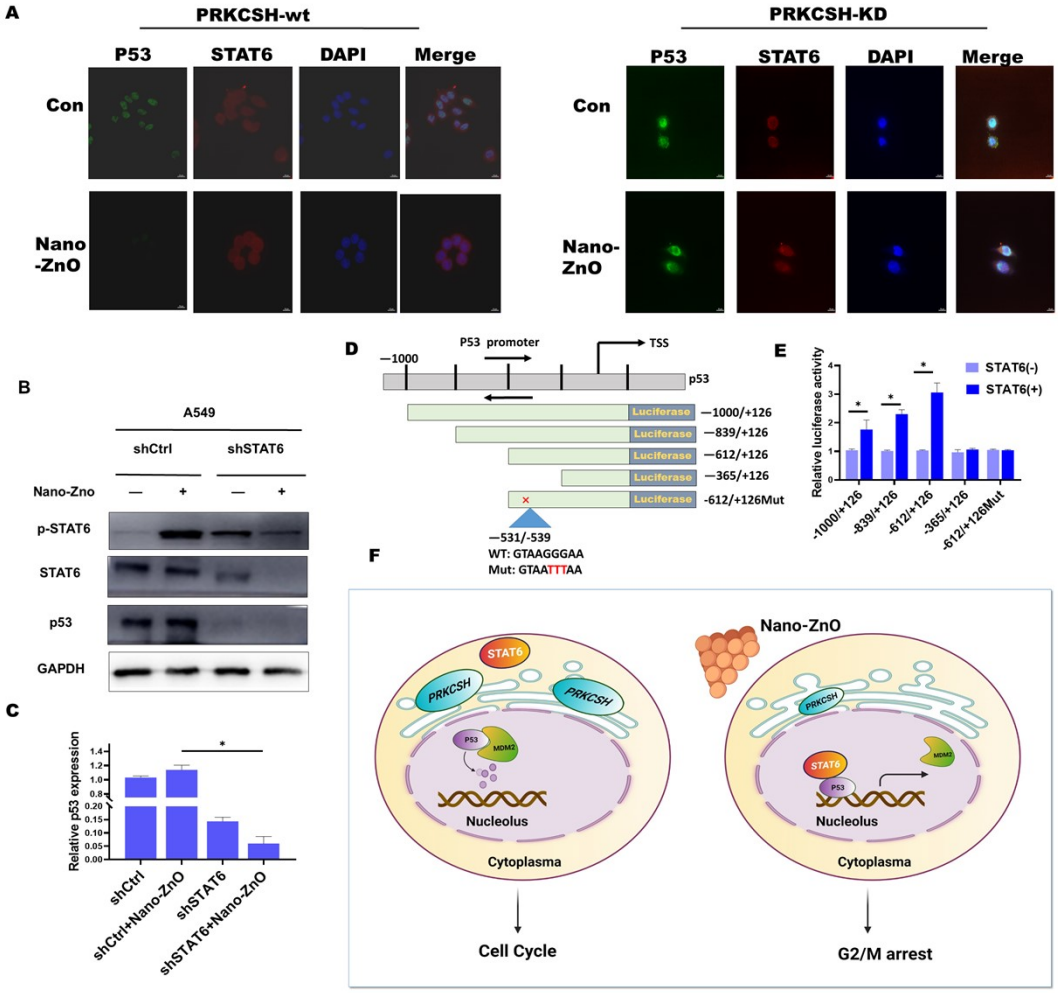

Figure 8. Direct regulation of p53 by STAT6. (A). Assay for the colocalization of p53 with STAT6. Immunocytochemical analysis of A549 cells expressing or not expressing PRKCSH and treated or not treated with 30 μg/mL Nano ZnO. Cells were immunostained with anti-p53 and anti-STAT6 antibodies. The scale bar represents 5 μm. Representative results (B) and

quantification (C) of p53 in A549 cells infected with shSTAT6 or control with/without 30 μg/mL Nano ZnO treatment. n = 3. (D). Schematic presentation of the p53 promoter with 5 potential STAT6 interaction elements. The reporter construct p53-Luc and its truncated and mutated derivatives are also shown. € The relative luciferase activity of deletion mutants and STAT6 interaction element mutants of p53-luc in A549 cells treated with 30 μg/mL Nano ZnO for 6 h. GAPDH served as the internal control. The data are presented as the means ± standard deviations (SDs) from three independent experiments; *p< 0.05 between different groups. (F). A schematic model for the mechanisms of PRKCSH in the regulation of the G2/M phase in A549 cells.

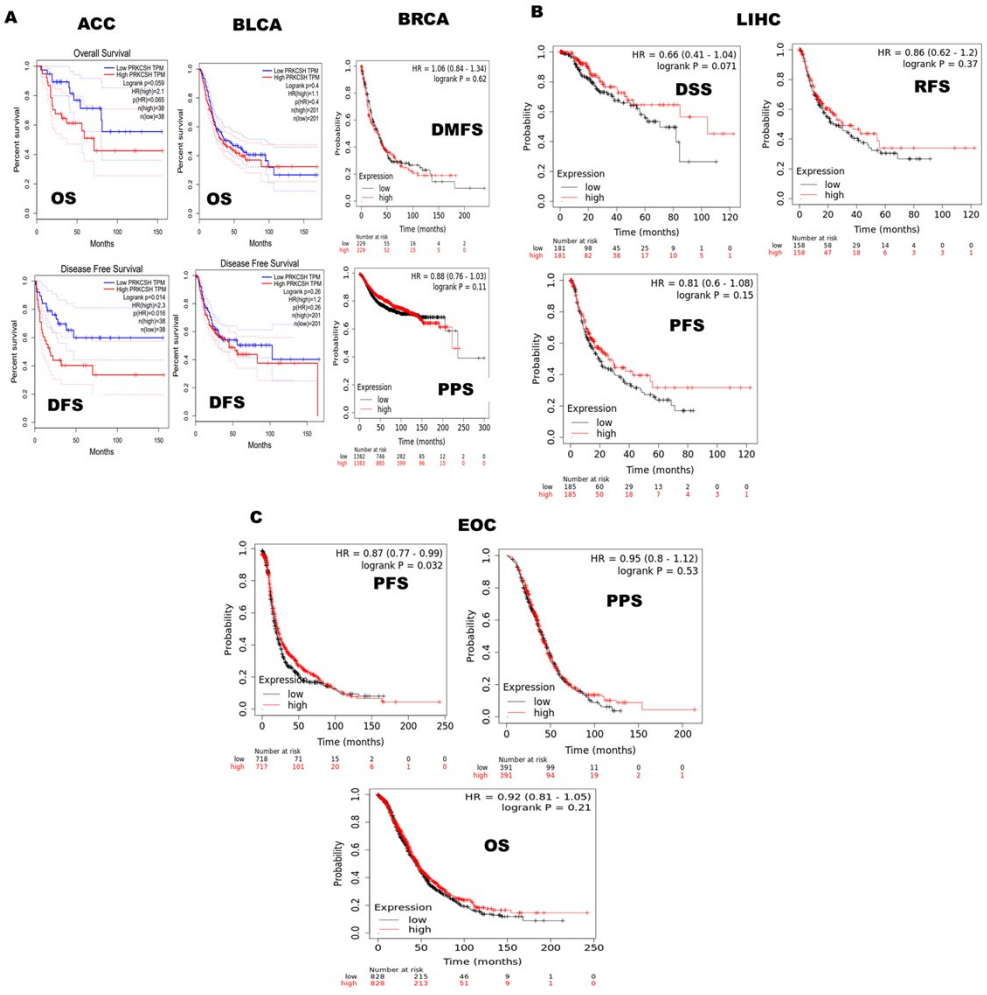

Supplementary Figure 1. **Kaplan–Meier survival curve analysis of the prognostic significance of high and low expression of PRKCSH in different types of human cancers using the Kaplan–Meier plotter database**. (A). Disease-free survival curves for adrenocortical carcinoma (ACC) patient groups with high and low PRKCSH expression

levels and bladder urothelial carcinoma (BLCA) and the distant metastasis-free survival (DMFS) and postprogression survival (PPS) of breast invasive carcinoma (BRCA) patient groups with high and low PRKCSH expression levels. (B), and PFS, PPS and OS for EOC patients (C). The data were obtained from TCGA datasets. The significance of the differences between the two categories was determined by a log-rank test. For comparative analysis between two groups, one-way ANOVA was used. Data are represented as the mean ± SEM of four samples; *p< 0.01. OS, overall survival; RFS, relapse-free survival; FP, first progression.

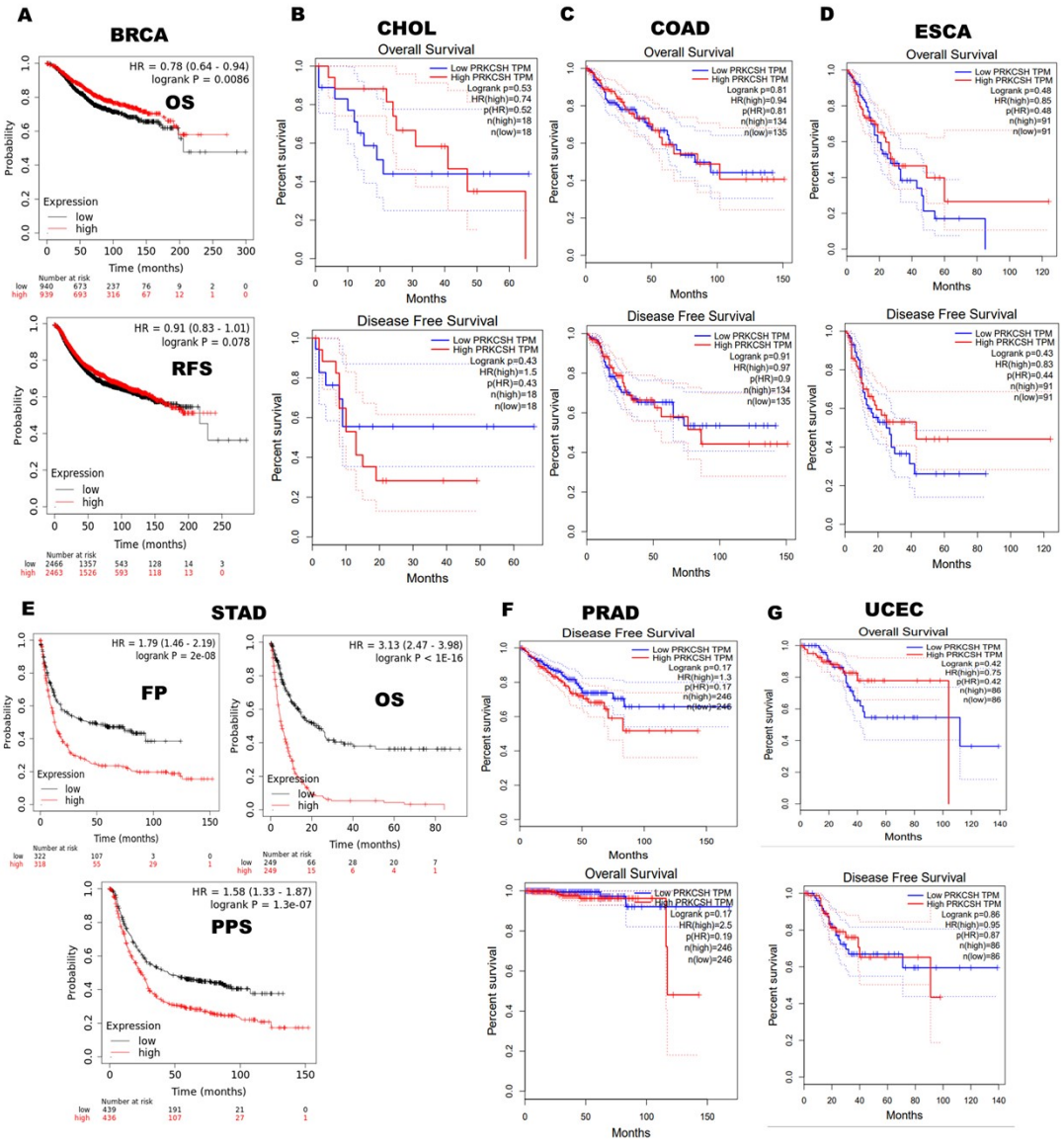

Supplementary Figure 2. **Kaplan–Meier survival curve analysis of the prognostic significance of high and low expression of PRKCSH in different types of human cancers using the Kaplan–Meier plotter database**. OS and RFS for patient groups with high and

low PRKCSH expression levels for BRCA patients (A), CHOL patients (B), COAD patients (C), and ESCA patients (D), and FP, OS and PPS for STAD patients (E), PRAD patients (F), and UCEC patients (G). The data were obtained from TCGA datasets. The significance of the differences between the two categories was determined by a log-rank test. For comparative analysis between two groups, one-way ANOVA was used. Data are represented as the mean ± SEM of four samples; *p< 0.01. OS, overall survival; RFS, relapse-free survival; PPS, postprogression survival; FP, first progression.

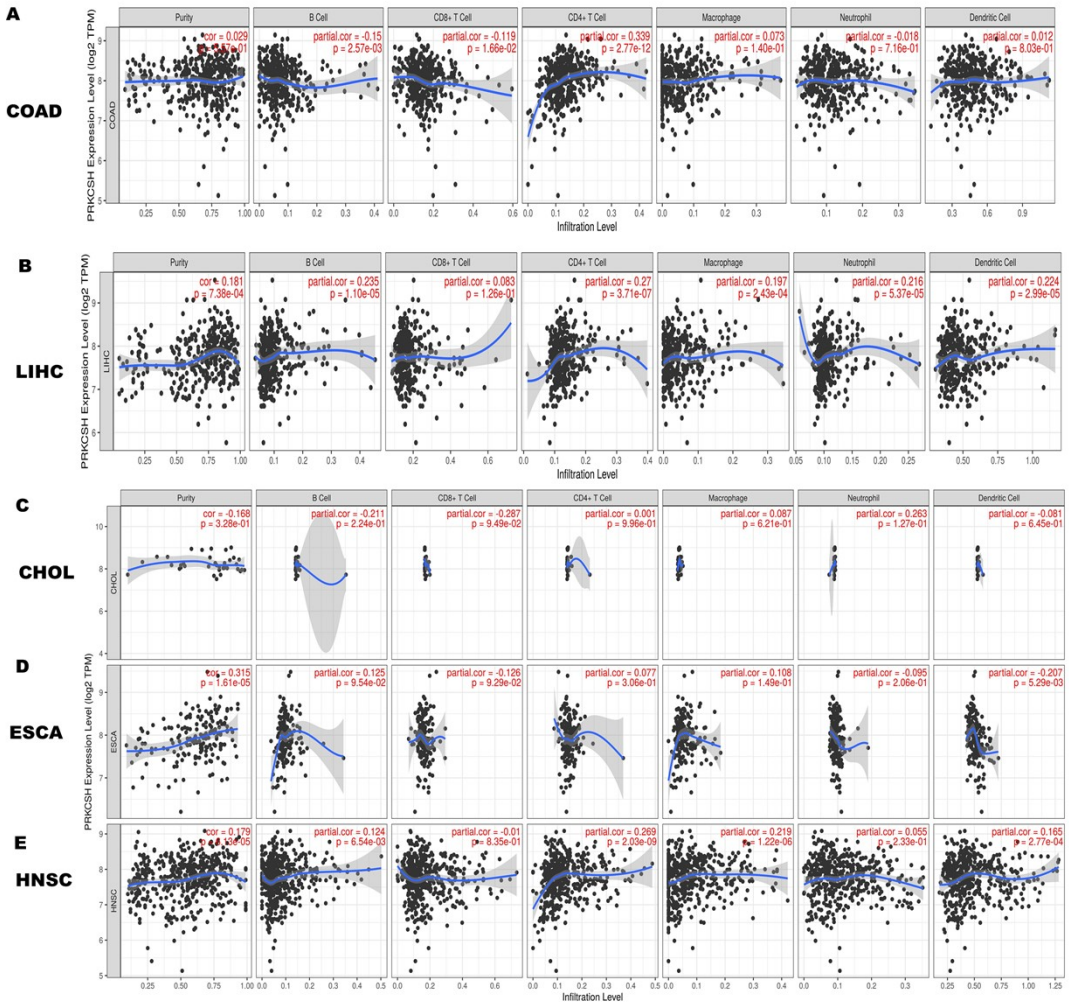

Supplementary Figure 3. Correlation analysis of PRKCSH expression and infiltration levels of immune cells in COAD (A), LIHC (B), CHOL (C), ESCA (D) and HNSC (E) tissues using the TIMER database. PRKCSH expression in cancer tissues positively correlates with tumour purity and infiltration levels of B cells, CD8+ T cells, CD4+ T cells, macrophages, neutrophils, and dendritic cells. Scatterplots will be generated and displayed after inputs are submitted successfully, showing the purity-corrected partial Spearman's rho value and

statistical significance. The gene expression levels against tumour purity are always displayed in the left-most panel.

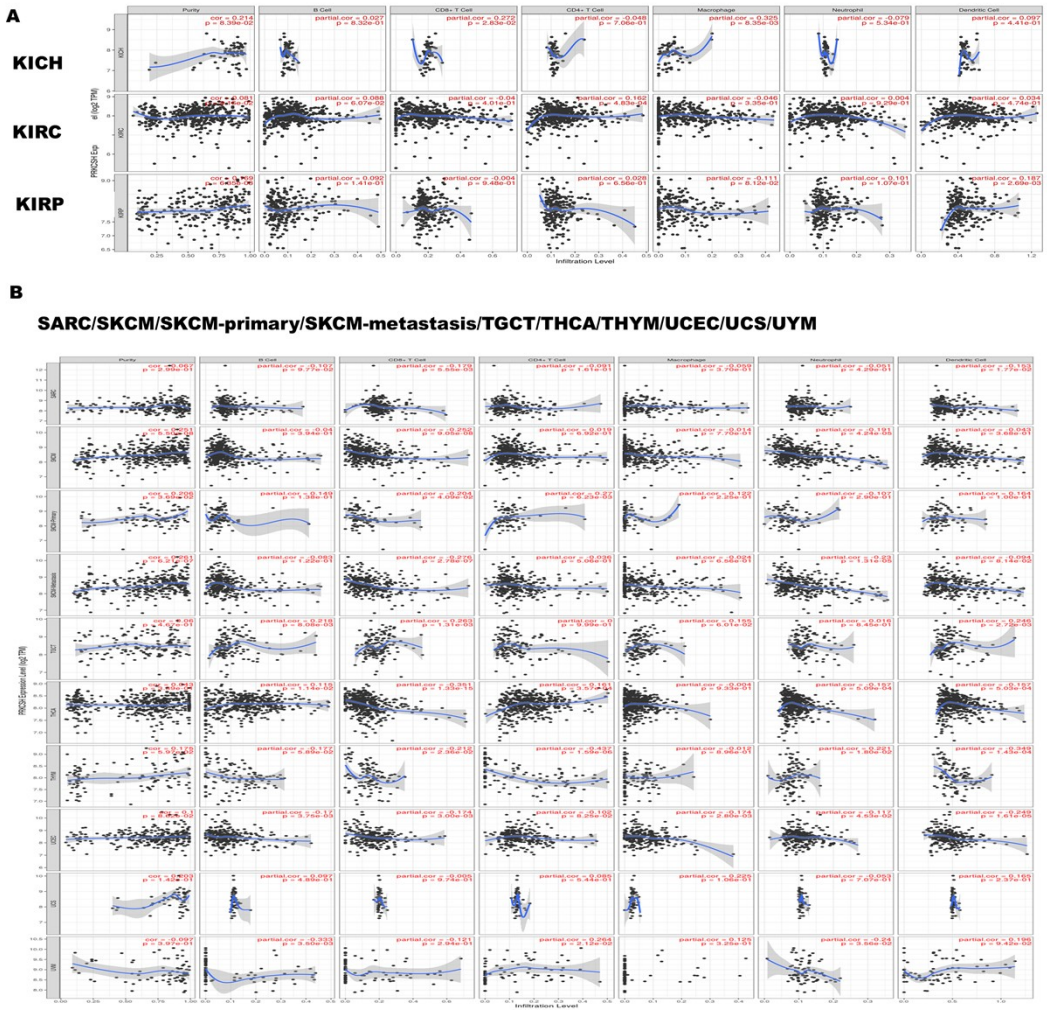

Supplementary Figure 4. Correlation analysis of PRKCSH expression and infiltration levels of immune cells in KICH/KIRC/KIRP (A) and SARC/SKCM/SKCM-primary/SKCM-metastasis/TGCT/THCA/THYM/UCEC/UCS/UYM (B) tissues using the TIMER database. PRKCSH expression in cancer tissues positively correlates with tumour purity and the infiltration levels of B cells, CD8+ T cells, CD4+ T cells, macrophages, neutrophils, and dendritic cells. Scatterplots will be generated and displayed after inputs are submitted successfully, showing the purity-corrected partial Spearman's rho value and statistical significance. The gene expression levels against tumour purity are always displayed in the left-most panel.

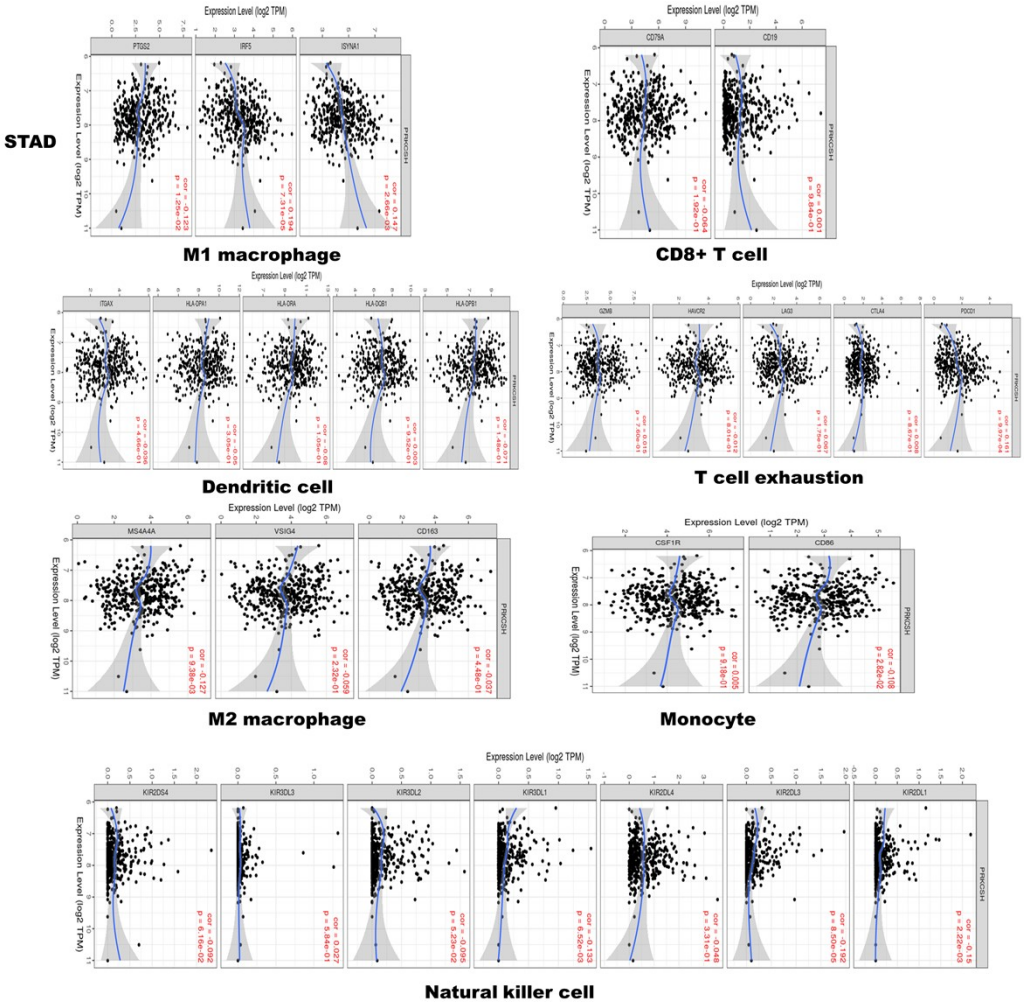

Supplementary Figure 5. Correlation analysis of PRKCSH expression and infiltration levels of immune cells in STAD tissues using the TIMER database. PRKCSH expression in cancer tissues positively correlates with tumour purity and infiltration levels of B cells, CD8+ T cells, CD4+ T cells, macrophages, neutrophils, and dendritic cells. Scatterplots will be generated and displayed after inputs are submitted successfully, showing the purity-corrected partial Spearman's rho value and statistical significance. The gene expression levels against tumour purity are always displayed in the left-most panel.

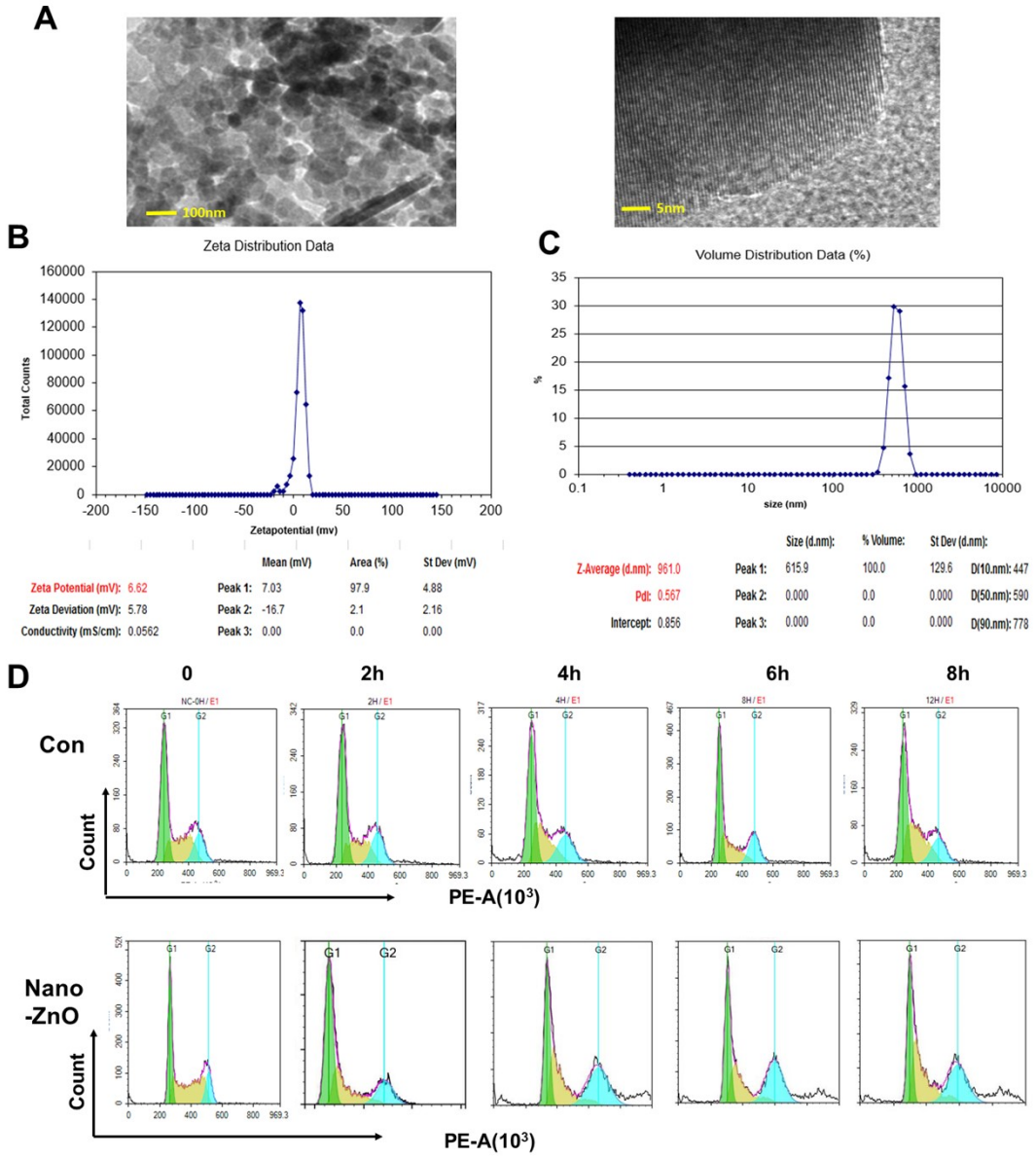

Supplementary Figure 6. (A) The mean diameter of Nano ZnO at a power of 20 nm was determined by TEM. (B) Mean zeta potential (mV) and (C) mean Z-average. (D). Representative flow cytometry histogram of cell cycle progression in the population of A549 cancer cells with or without 30 µg/ml Nano ZnO treatment.

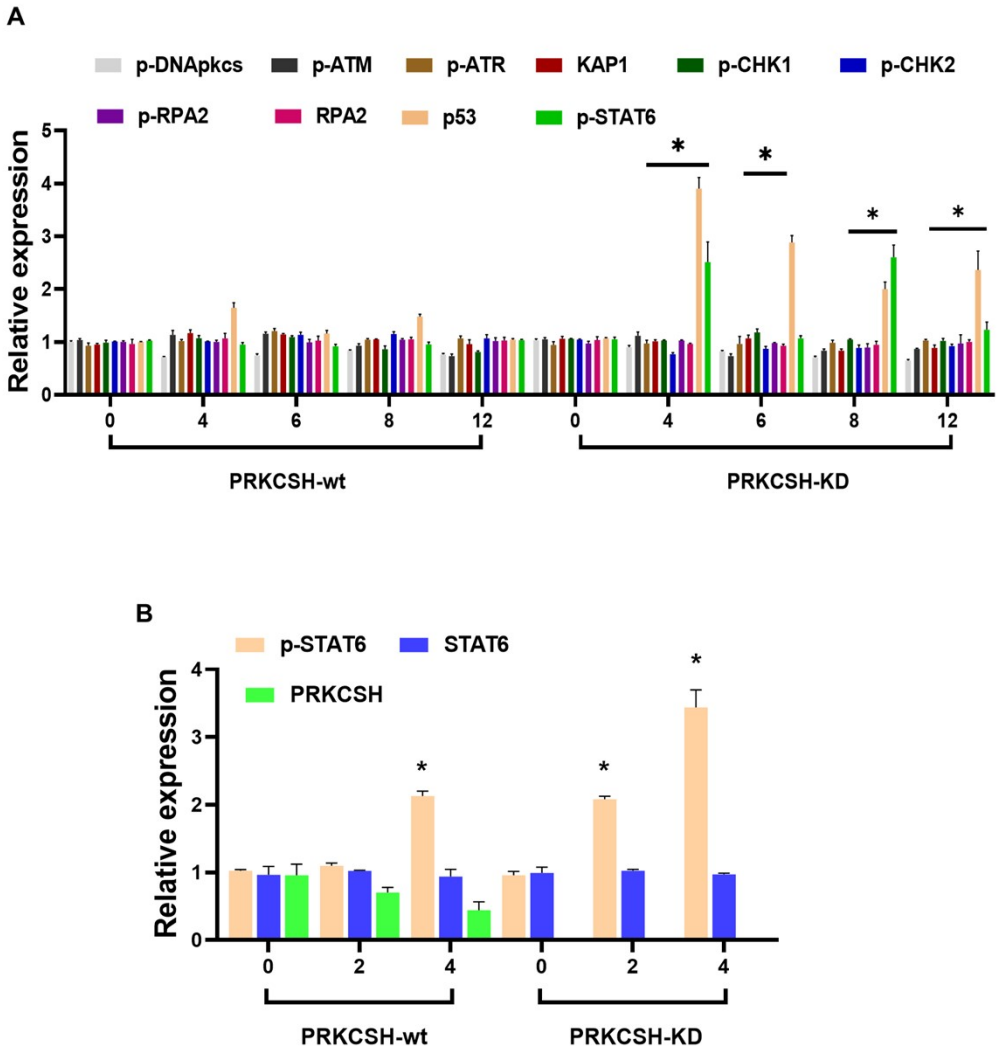

Supplementary Figure 7. (A) Quantitative measurement of G2/M checkpoint-regulating proteins and DNA damage proteins (pDNApkcs, pATM, pATR, KAP1, p-CHK1, p-CHK2, p-RPA2, RPA2, p53, and p-STAT6) in Nano-ZnO-treated PRKCSH-WT and PRKCSH-KD A549 cancer cells.

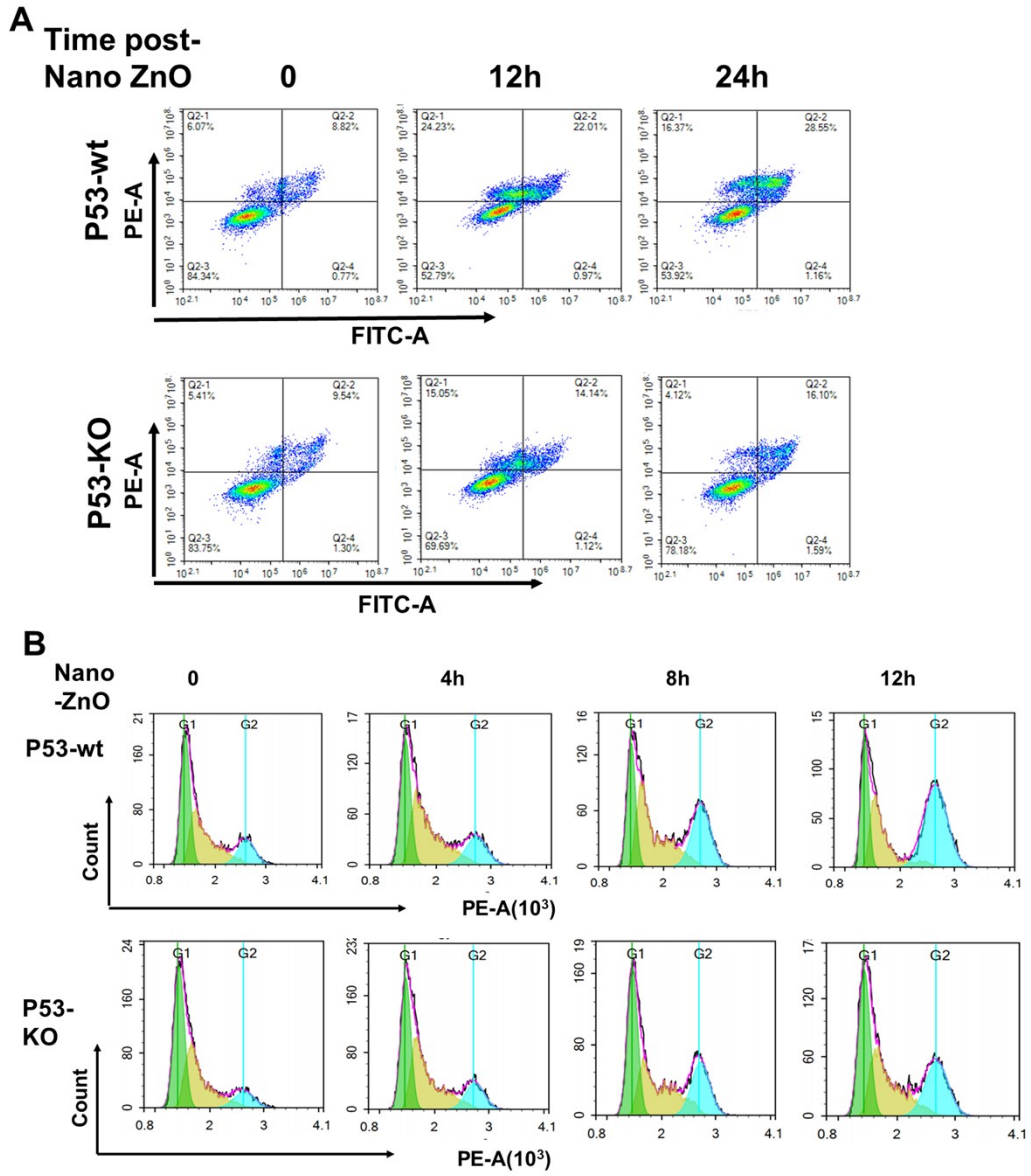

Supplementary Figure 8. (A) Effects of Nano ZnO on apoptosis in A549 cancer cells with or without p53 after treatment with 30 μg/ml Nano ZnO. (B) Effects of Nano ZnO on the cell cycle in A549 cancer cells with or without p53 after treatment with 30 μg/ml Nano ZnO.

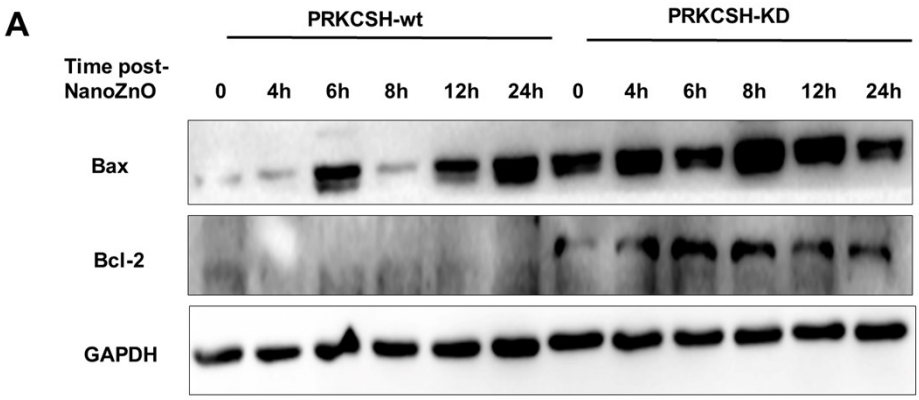

Supplementary Figure 9. (A) Effects of Nano ZnO on Bax and Bcl-2 expression in A549 cancer cells with or without PRKCSH after treatment with 30 μg/ml Nano ZnO.